AD-A140 013 THE EFFECTS OF DIELECTRIC AND SOIL NONLINEARITIES ON THE EMP RESPONSE OF..(U) ELECTRO MAGNETIC APPLICATIONS INC ALBUQUERQUE NM R A PERALA ET AL. FEB 83 1/1

UNCLASSIFIED HDL-CR-83-132-1 DAAG39-78-C-0132 F/G 20/14 NL

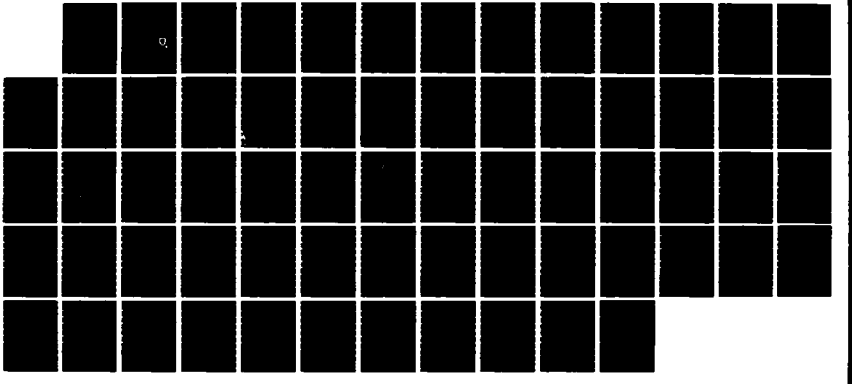

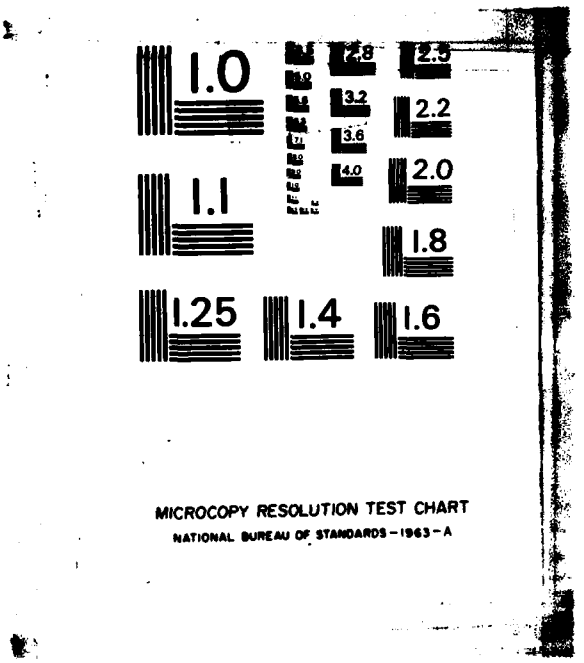
1.0
1.1
1.25
1.4
1.6
2.8
3.2
3.6
4.0
2.5
2.2
2.0
1.8
MICROCOPY RESOLUTION TEST CHART
NATIONAL BUREAU OF STANDARDS - 1963 - A

HDL-CR-83-132-1

February 1983

The Effects of Dielectric and Soil Nonlinearities on the EMP Response of Cables Lying on the Surface of the Earth

R. A. Perala
R. B. Cook

Prepared by

Electro Magnetic Applications, Inc.
1025 Hermosa Blvd., SE, P.O. Box 8482
Albuquerque, NM 87198

Under contract

DAAG39-78-C-0132

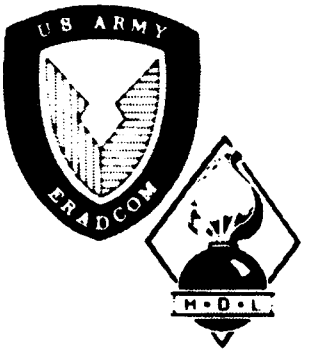

U.S. Army Electronics Research and Development Command
Harry Diamond Laboratories
Adelphi, MD 20783

The findings in this report are not to be construed as an official Department of the Army position unless so designated by other authorized documents.

Citation of manufacturers' or trade names does not constitute an official indorsement or approval of the use thereof.

Destroy this report when it is no longer needed. Do not return it to the originator.

UNCLASSIFIED

SECURITY CLASSIFICATION OF THIS PAGE (When Data Entered)

REPORT DOCUMENTATION PAGE

READ INSTRUCTIONS BEFORE COMPLETING FORM

1. REPORT NUMBER: HDL-CR-83-132-1
2. GOVT ACCESSION NO.: AD-A140
3. RECIPIENT'S CATALOG NUMBER: 013

4. TITLE (and Subtitle): The Effects of Dielectric and Soil Nonlinearities on the EMP Response of Cables Lying on the Surface of the Earth

5. TYPE OF REPORT & PERIOD COVERED: Contractor Report

6. PERFORMING ORG. REPORT NUMBER:

7. AUTHOR(s): R. A. Perala, R. B. Cook — HDL Contact: William Scharf

8. CONTRACT OR GRANT NUMBER(s): DAAG39-78-C-0132

9. PERFORMING ORGANIZATION NAME AND ADDRESS: Electro Magnetic Applications, Inc., 1025 Hermosa Blvd., SE, P.O. Box 8482, Albuquerque, NM 87198

10. PROGRAM ELEMENT, PROJECT, TASK AREA & WORK UNIT NUMBERS: Program Element: 62704H

11. CONTROLLING OFFICE NAME AND ADDRESS: Harry Diamond Laboratories, 2800 Powder Mill Road, Adelphi, Maryland 20783

12. REPORT DATE: February 1983

13. NUMBER OF PAGES: 65

14. MONITORING AGENCY NAME & ADDRESS (if different from Controlling Office):

15. SECURITY CLASS. (of this report): UNCLASSIFIED

15a. DECLASSIFICATION/DOWNGRADING SCHEDULE:

16. DISTRIBUTION STATEMENT (of this Report)

Approved for public release; distribution unlimited.

17. DISTRIBUTION STATEMENT (of the abstract entered in Block 20, if different from Report)

18. SUPPLEMENTARY NOTES

HDL Project: E050E3
DRCMS Code: 36AA.6000.62704

19. KEY WORDS (Continue on reverse side if necessary and identify by block number)

EMP
Source region
Coupling
Dielectric breakdown

20. ABSTRACT (Continue on reverse side if necessary and identify by block number)

Analytic evaluation of "typical" Army cables demonstrates that coupling due to nuclear source-region EMP is sufficient to cause dielectric breakdown of the cable jacket dielectric, the air surrounding the cable, and, in some cases, the soil itself. The result of these nonlinearities is to greatly increase the late-time current that can be coupled into systems. The report presents the current waveforms induced on RG-8 and RG-58 cables exposed to high-altitude and source-region EMP environments over lengths of 100, 600, and 280 m. Experiments are suggested for validating some of the code assumptions.

DD FORM 1 JAN 73 1473 EDITION OF 1 NOV 65 IS OBSOLETE

UNCLASSIFIED

TABLE OF CONTENTS

LIST OF ILLUSTRATIONS

LIST OF TABLES

SECTION 1

INTRODUCTION

When a cable lying on the surface of the earth is exposed to an electromagnetic pulse from a nuclear burst, currents are induced on the cable. These currents can be on the order of a few hundred to a few thousand amperes, depending upon such things as soil conductivity, cable dimensions, terminations, and angle of incidence. Surface cables are used to connect various types of tactical equipment, and cable responses of this magnitude may possibly upset or damage electronic circuits in these equipments.

Linear analysis [1-4] of surface cable response to both high altitude and tactical EMP environments predict voltage levels that may be sufficient to break down cable dielectrics. In addition, the predicted potential gradient across the soil surface is large enough to cause soil breakdown. The significance of the effect nonlinearities have on the current coupled to surface cables must be determined and, if found to be significant, must be incorporated into the coupling codes used for surface system EMP studies.

Nonlinear cable analysis tools have recently been developed for buried cables [5-7]. One such tool is the computer code BLINE which was written and used to predict these effects. The BLINE results for buried cables have shown that the breakdown of soil and cable dielectric can have an effect on the induced cable currents. The general intent of this study, therefore, is to do a similar investigation into the effects of nonlinearities on surface cable response.

Specifically, the study has the following three objectives:

(1) Identify and document all nonlinear parameters associated with the coupling of EMP energy to Army system-type cables when they are exposed to "close-in" tactical nuclear environments.

(2) Determine and document the importance of these nonlinear parameters in terms of their significance to the magnitude of energy delivered to system electronics for "close-in" EMP coupling situations.

(3) Consider and document simple experiments that may be used to illustrate the nonlinear effects of voltage on cable and soil parameters used in calculating the coupling of EMP fields to surface cables exposed to "close-in" tactical EMP environments.

In view of the above objectives, four different tasks were addressed:

(1) Modification of BLINE to compute surface cable response.

(2) Computation of linear and nonlinear responses for specific cables.

(3) Determination of the need for treatment of nonlinear air conductivity.

(4) Determination of the feasibility of using high level EMP simulators, such as AESOP or TEMPS to demonstrate the expected nonlinear response of standard cables.

In the remainder of the report, modifications of BLINE will first be addressed. Then the computational results for the linear and nonlinear cases will be discussed. Then the feasibility of certain experiments will be demonstrated. Finally, conclusions will be made along with recommendations for further investigations.

SECTION 2

MODIFICATIONS OF BLINE TO COMPUTE SURFACE CABLE RESPONSE

2.1 Background

BLINE is a computer code developed by EMA personnel which solves the nonlinear response of cables buried in the earth. A complete description of BLINE can be found in Reference 5, but a summary will be given here to provide enough background in order to help the reader understand the modifications necessary to make it a surface cable code.

There are several analysis tools used to predict the response of buried cables to EMP. All of the models used reduce the problem to an equivalent transmission line (Figure 2.1). In the equivalent transmission line model the current I flowing on the metal conductor is related to the voltage V between the conductor and a distant reference point by the telegraphers' equations:

$$\frac{\partial V(z,\omega)}{\partial z} = -Z(\omega)I(z,\omega) + E_z^{inc}(z,\omega) \tag{2.1}$$

and

$$\frac{\partial I(z,\omega)}{\partial z} = -Y(\omega)\,V(z,\omega) + I_s(z,\omega). \tag{2.2}$$

Here ω is the fourier transform variable, $Z(\omega)$ and $Y(\omega)$ are the incremental impedance and admittance of the equivalent line, and E^{inc} and I_s are the incident electric fields and impressed current density (as from a lightning stroke). Because these parameters account for the presence of both the cable dielectric and the soil, any simple equivalent (Figure 2.1b) must have elements that are complex functions of frequency. For the more accurate frequency domain treatment, the incremental parameters are determined from the characteristic impedance and propagation constant of the TM_0 mode as

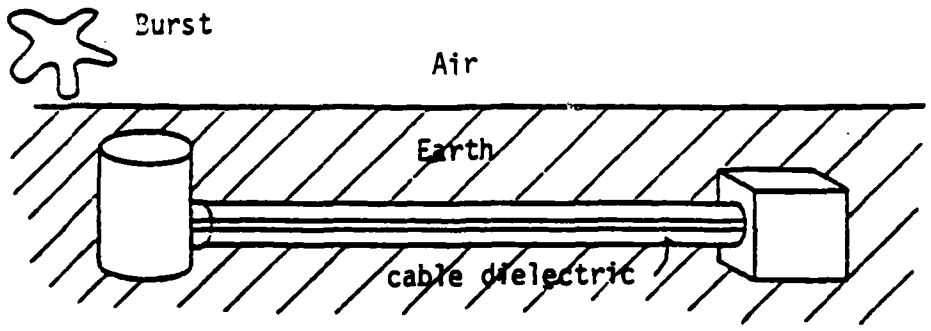

a. Original Buried Cable Problem

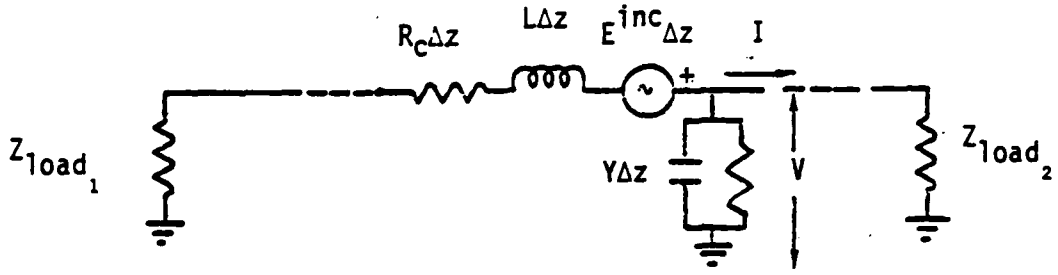

b. Two-Equation Transmission Line Equivalent

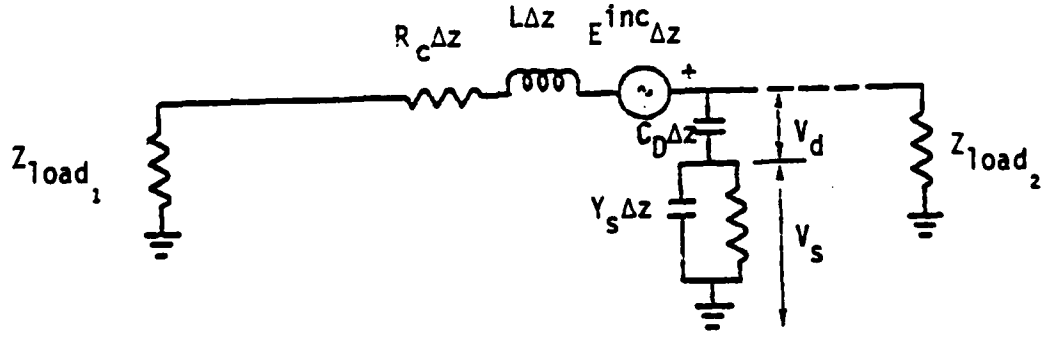

c. Three-Equation Transmission Line Equivalent

Figure 2.1 Modeling Buried Conductor Problem

$$Z = -j\gamma Z_c \quad \text{and} \quad Y = \frac{-j\gamma}{Z_c}, \tag{2.3}$$

where the propagation constant γ and characteristic impedance Z_c is solved by finding zeros of a complicated transcendental equation [3]. For more approximate frequency domain solutions and time domain approaches, the use of three telegraphers' equations is more appropriate [8]:

$$\frac{\partial(V_d + V_s)}{\partial z} = -Z(\omega)I(z,\omega) + E^{inc}(z,\omega) \tag{2.4}$$

$$\frac{\partial I}{\partial z} = -Y_d(\omega)\, V_d(z,\omega) + I_s(z,\omega) \tag{2.5}$$

$$\frac{\partial I}{\partial z} = -Y_s(\omega)\, V_s(z,\omega) + I_s(z,\omega). \tag{2.6}$$

In this formulation the parameters Y_d and Y_s are more easily determined from known solutions to simpler problems:

$$Y_d(\omega) \stackrel{def}{=} G_d + j\omega C_d = \frac{2\pi\sigma_d}{\ell n\left(a_2/a_1\right)} + j\omega\frac{2\pi\epsilon_d}{\ell n\left(a_2/a_1\right)} \tag{2.7}$$

$$Z(\omega) \stackrel{def}{=} R_c + j\omega L = R_c + j\omega\left[\frac{\mu_0}{2\pi}\ell n\left(a_2/a_1\right) + \frac{\mu_0}{2\pi}\ell n\left(a_3/a_2\right)\right] \tag{2.8}$$

$$Y_s(\omega) \stackrel{def}{=} G_s + j\omega C_s = \frac{2\pi\sigma_s}{\ell n\left(a_3/a_2\right)} + j\omega\frac{2\pi\epsilon_s}{\ell n\left(a_3/a_2\right)}. \tag{2.9}$$

Here

R_c is the DC resistance of the cable conductor,

a_1 is the radius of the cable conductor,

a_2 is the outer radius of the dielectric sheath,

a_3 is a third characteristic dimension that depends upon the frequency of excitation.

Following Vance [9] one would use

$$a_s = \frac{\sqrt{2}\,\delta}{1.781} = .794\,\delta \tag{2.10}$$

The time domain equivalent of the telegraphers' equations for the three equation models are:

$$\frac{\partial(V_d+V_s)}{\partial z} = -L\,\frac{\partial I}{\partial t} - R_c I + E^{inc}(z,t) \tag{2.11}$$

$$\frac{\partial I}{\partial z} = -C_d\,\frac{\partial V_d}{\partial t} - G_d V_d + I_s(z,t) \tag{2.12}$$

$$\frac{\partial I}{\partial z} = -C_s\,\frac{\partial V_s}{\partial t} - G_s V_s + I_s(z,t). \tag{2.13}$$

Here, the values of R_c, L, C_d, C_s, and G_s are taken from equations 2.7, 2.8, and 2.9 where the outer radius parameter a_s is not time dependent. It is noted that selecting any constant value overestimates the inductance (underestimates the induced current) at early time ($t < t_d$) and underestimates the inductance (overestimates the induced current) at late times ($t < t_d$), where t_d is determined from a_s using:

$$a_s \simeq \frac{\sqrt{2}\delta}{1.781} = \frac{\sqrt{2}}{1.781}\sqrt{\frac{t_d}{\mu_0 \sigma_{soil}}}\,. \tag{2.14}$$

2.2 Modifications to BLINE to Handle Surface Cables

Because BLINE was written for cables completely buried in the earth, it must be modified to treat cables lying on the earth's surface. Both linear and nonlinear aspects must be taken into account.

Modifications for the linear aspect, which for our purposes will include the effects of time varying air conductivity, involve modification of the per unit length impedance and admittance parameters. For a cable buried in soil, the parameters may be written

$$\begin{aligned} Z_s &= R_c + j\omega L_s \\ Y_s &= G_s + j\omega C_s \end{aligned} \tag{2.15}$$

Where

$$L_s = \frac{\mu_0}{2\pi} \ln \frac{.794\ \delta_s}{a_1}$$

$$C_s = \frac{2\pi \varepsilon_s}{\ln \frac{.794\ \delta_s}{a_2}} \quad ; \quad G_s = \frac{\sigma_s}{\varepsilon_s} C_s \qquad (2.16)$$

In the above, the subscript s refers to the soil medium, and δ_s is the skin depth in the soil given by

$$\delta_s(\omega) = \sqrt{\frac{2}{\omega \mu_0 \sigma_s}} \qquad (2.17)$$

In order to convert to the time domain, the approximation is made that $t = 2/f$ [5], so that

$$\delta_s(t) \cong \sqrt{\frac{t}{2\pi\ \mu_0 \sigma_s}} \qquad (2.18)$$

Here, t is measured from the time that an excitation arrives at the location of interest.

In an infinite time varying conducting air medium having conductivity $\sigma_A(t)$, formulas analagous to those for soil above can be obtained merely by replacing the subscript s by A.

The final result for a cable on the surface is then the combination of the above results:

$$Z_{surface} = \frac{2Z_A(t)Z_s(t)}{Z_A(t) + Z_s(t)}$$

$$Y_{surface} = \frac{1}{2}\left(Y_A(t) + Y_s(t)\right) \qquad (2.19)$$

These formulas then define the equivalent surface cable per unit length impedance and admittance including the effects of time varying air conductivity. They can also be applied to the case $\sigma_A = o$, for which the limit is

$$Z_{surface} \cong 2Z_s(t)$$

and

$$Y_{surface} \cong \frac{1}{2} Y_s(t) \tag{2.20}$$

It is noted that this results in the propagation constant of the surface cable (in the presence of nonconducting air) being equal to that of a buried cable, and the characteristic impedance of the surface cable being twice that of a buried cable.

In addition to modifying the soil parameters for the linear case, the dielectric admittance must also be modified. For the buried cable, the dielectric capacitance is simply that of a coaxial cable formed by the soil and conductor boundaries. The same is true if the cable is at the interface between two conducting media such as conducting air and soil. However, as the air conductivity approaches zero, the radial electric field lines on the conductor all terminate on the soil and are not azimuthally uniform about the conductor.

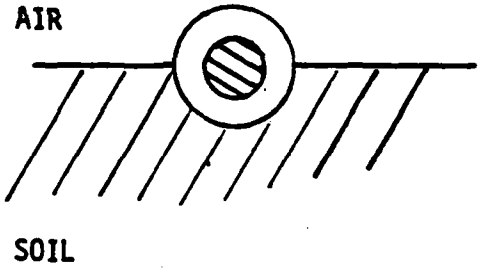

Figure 2.2 Geometry Used to Calculate Soil Per Unit Length Impedances and Admittances, and Cable Dielectric Admittance for Conducting Air.

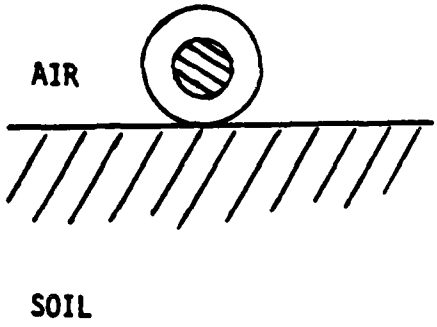

Figure 2.3 Geometry Used to Calculate Cable Dielectric Admittance for HAB Case.

Thus, for the time varying conducting air medium above the soil, the geometry of Figure 2.2 can be used to compute all cable parameters.

However, for no air conductivity (the HAB case), the situation is somewhat different. A surface cable would not be deployed in the manner of Figure 2.2, although that is the correct model for source region computations. (In the presence of conducting air, the radial field lines should be azimuthally uniform, even if deployed like Figure 2.3.) A surface cable would be more nearly deployed in the manner of Figure 2.3. It is clear that in this case, the dielectric capacitance is determined by the geometry of a wire over a ground plane. This also means that the radial electric field is not simply that given by coaxial geometry as in the BLINE case, but is given by the wire over a ground plane geometry, Figure 2.3. The electric field is therefore a maximum on the soil side of the conductor, and minimum on the top.

The nonlinear aspect of BLINE to be modified for surface cables involves the treatment of soil breakdown, whereas the dielectric breakdown is unmodified, that is, dielectric breakdown is treated as a hard short.

For a cable buried in the soil, the ionized soil region is roughly spherical (except for a bicone coaxial with the cable) and the radius is determined by the soil breakdown electric field, which is 1-2MV/m. For a cable on the surface of the earth, an arc to the earth will form a region roughly the shape of a thin disc, because the surface breakdown of soil (250-500 kV/m) is much less than that of the bulk soil medium. Therefore, the ionized region tends to extend along the earth's surface instead of into it [10].

The ionized region is treated as a thin disc of radius r_{arc}, where r_{arc} increases until the electric field at the edge of the disc is equal to the surface breakdown field E_{BR}. For a current I flowing into the disc, r_{arc} is determined by

$$E_{BR} = \frac{I}{4\sigma_s r_{arc}^2} \tag{2.21}$$

from which one obtains

$$r_{arc} = \sqrt{\frac{I}{4\sigma_s E_{BR}}} \tag{2.22}$$

The disc then has a conductance G_{arc} and capacitance C_{arc} given by

$$\begin{aligned} G_{arc} &= 4\sigma_s r_{arc} \\ C_{arc} &= 4\varepsilon_s \cdot r_{arc} \end{aligned} \tag{2.23}$$

The relationship of the conducting disc to the TEM transmission line surface cable code is illustrated in Figure 2.4. In order to ensure that r_{arc} is never greater than one-half the spatial increment Δz, r_{arc} is set equal to the smaller of $\Delta z/2$ or r_{arc}.

It is noted that the soil may break down before the cable dielectric does. When the dielectric punctures, current flows through the puncture into the soil forming a disc as previously described. However, when the soil breaks down and the dielectric does not, the concept of the disc does not apply because the current flowing into the soil is distributed along the cable length and does not flow from a discrete point. In this case, the soil nonlinearity is treated differently as discussed in the following.

The cable geometry of Figure 2.2 is assumed. The ionized soil region will then extend into the soil a radius of a_2 until the electric field is equal to the bulk breakdown field of the soil. This breakdown field is then given by

$$E_{BR} = \frac{V_{soil}}{a_2 \ln \frac{a_1}{a_2}} \tag{2.24}$$

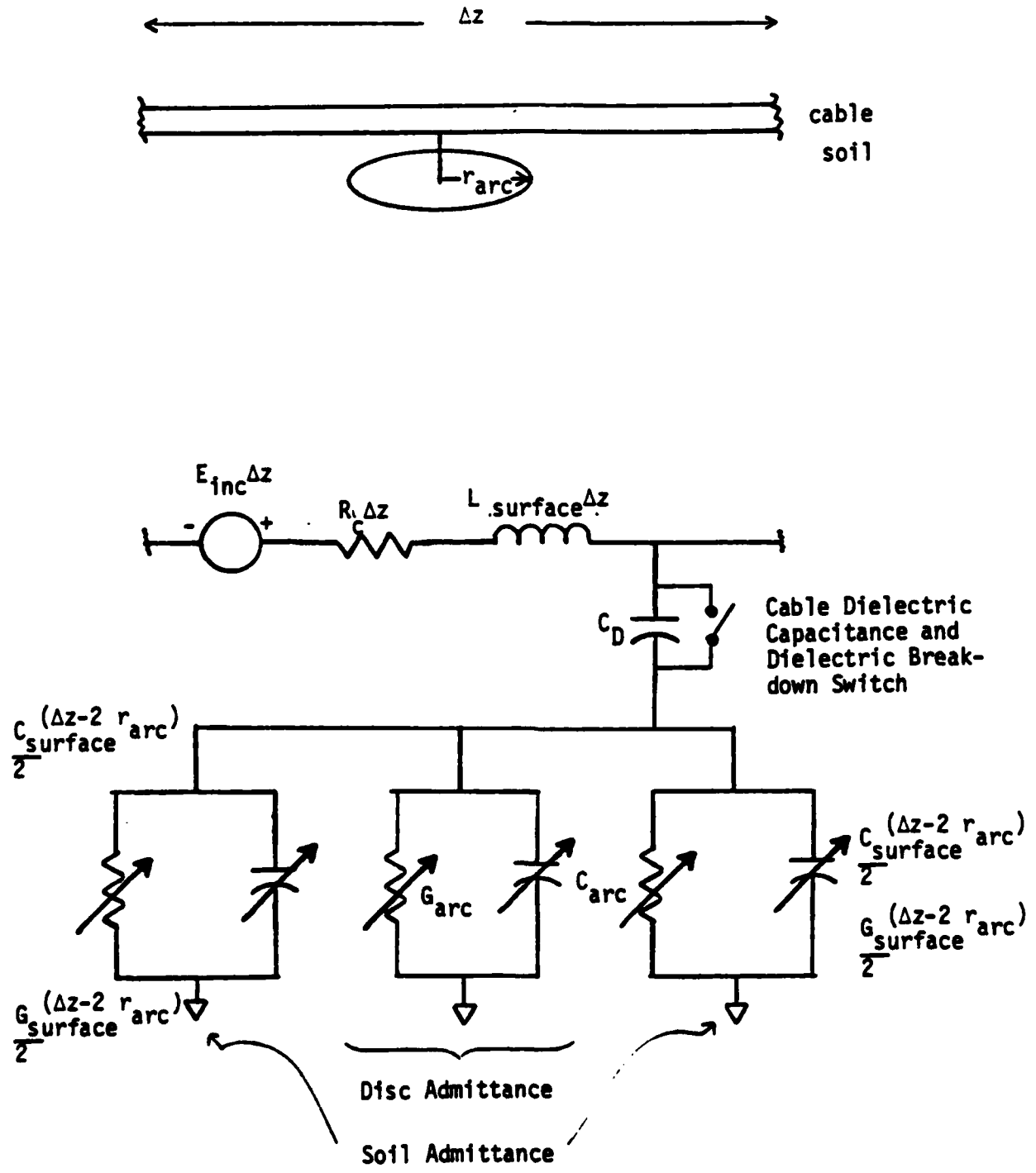

Figure 2.4 Illustration of Surface Cable Soil Breakdown and Incorporation into TEM Transmission Line Model.

This equation can then be solved for the new radius a_2^1. However, because it is a transcendental equation which must be solved at every time step (a time consuming process) an approximate solution is used:

$$a_2^1 = \frac{V_{soil}}{E_{BR} \ln \frac{a_3}{a_2^1}} \tag{2.25}$$

where a_2^1 on the left hand side is the new value and a_2^1 on the right hand side is the value obtained from the previous time step. The solution is started by letting a_2^1 initially be equal to a_2.

The computation of the electric field is also necessary in order to determine dielectric breakdown. For the coaxial case, the maximum electric field E_{max} in the dielectric having a potential V across it is given by

$$E_{max} = \frac{V}{a_1 \ln \frac{a_2}{a_1}} \tag{2.26}$$

For the wire over the ground plane case, it is given by

$$E_{max} = \frac{V}{\cosh^{-1} \frac{a_2}{a_1}} \left[\frac{1}{\frac{X+d}{2}} - \frac{1}{\frac{X-d}{2}} \right] \tag{2.27}$$

where $X = a_2 - a_1$

$$d = a_1 \left(K_1 - \frac{1}{K_1}\right)$$

$$K_1 = \frac{a_2}{a_1} \left(1 + \sqrt{1 - \left(\frac{a_1}{a_2}\right)^2}\right).$$

SECTION 3

RESULTS OF SURFACE CABLE COMPUTATIONS

3.1 Background

One of the goals of the study was to perform surface cable computations for several cases, with and without including the nonlinear effects. Table 3.1 summarizes the cables studied, the soil conductivities, and the environments used for the parameter study. Both linear and nonlinear predictions were made in order to ascertain the effects of including nonlinearities.

Table 3.1 Surface Cables for Parameter Study

Length	Environment	Soil Conductivity (mho/m)
100 m	HAB Overhead	.005
	HAB Overhead	.01
	Tactical EMP	.005
	Tactical EMP	.01
600 m	HAB Overhead	.005
	HAB Overhead	.01
	Tactical EMP	.005
	Tactical EMP	.01
2800 m	HAB Overhead	.005
	HAB Overhead	.01
	Direct Hit at End of Cable	.005
	Direct Hit at End of Cable	.01

The surface cables studied are formed by the shield and outer dielectric jacket of RG 58 and RG 8 cables, whose dimensions are indicated in Table 3.2.

Table 3.2 Dimensions of Cables Used in the Study [11].

Cable	a_1 (mm)	a_2 (mm)	Dielectric Thickness (mm)
RG 58	4.276	4.95	.674
RG 8	9.209	10.29	1.081

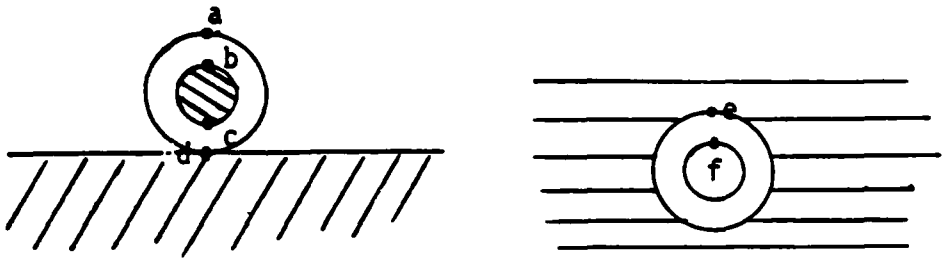

a. wire over a ground plane b. wire in conducting medium

Figure 3.1 Geometry for Definitions of Radial Electric Fields.

Table 3.3 Constants Used to Multiply the Dielectric Voltage to Obtain the Radial Electric Field at the Points Defined in Figure 3.1

Cable	E_a	E_b	E_c	E_d	E_e	E_f
RG 58	187	262	1670	1408	1276	1752
RG 8	92	118	1006	888	824	1043

The radial electric fields are computed by a constant which multiplies the dielectric voltages. Figure 3.1 and Table 3.3 define the constants at the locations indicated. When this constant is multiplied by the dielectric voltage, the result is the electric field at that location in volts/meter.

The cable jacket material is polyvinyl-chloride (PVC). In order to do the nonlinear computations, it was necessary to determine what the dielectric strength of PVC is. Several values were found in the literature and are summarized in Table 3.4. It is clear that values vary widely and depend upon the types of material, thickness tested, and test waveform. Values for polyethylene (PE) are included for reference

purposes. It is troublesome that the relative dielectric strength of PE and PVC varies considerably from source to source. The problem is compounded by the fact that for the purposes at hand, it is desireable to have a value which applies to a voltage which rises in a few hundred nanoseconds and is gone nominally within one or several microseconds, and probably none of the data in Table 3.4 applies to this time regime.

Table 3.4 Summary of PVC and PE Dielectric Strength Data from Various Sources. Units are volts/mil.

Source	PVC	PE
Reference 12	375	420-550
Reference 13	400	
Reference 14	600-1000 (flexible) 700-1300 (rigid)	460
Reference 15	800-1000	460
Reference 16	800 (AC) 2000 (DC)	1200 (AC) 3000 (DC)

Extensive data has been taken on PE breakdown and is summarized in Reference 17. This data shows that for lightning type pulses (1½ x 40 μsec), a conservative value to use is 2000 V/mil. It should be noted that some data exists for even shorter pulses (1 x 5 μsec) which yield a 5000 V/mil value [18]. A value of 2000 V/mil was used in other buried cable studies [5]. If one assumes PVC behaves similarly to PE and uses the data from Reference 16, one obtains a value of 1330 volts/mil for PVC. It is admitted that this is a guess based on conflicting data, and if one is going to perform some experiments involving cable breakdown, one should first obtain the dielectric strength data for the time regime of interest. It is noted that cable manufacturers were called, but they have no data on the jacket dielectric strength.

3.2 Computations for the High Altitude Burst (HAB)

The threat for the HAB predictions was taken to be a plane wave normally incident upon the earth and polarized parallel to the cable. Previous work which investigated angle of incidence effects showed that end-on incidence results in only one-half the response of normal incidence [3], and responses for other angles of incidence yields values within one percent of the normal incident case, so it is felt that normal incidence is the appropriate case to study. The temporal behavior of the plane wave is the familiar double exponential

$$E_{inc} = 52\ (e^{-4x10^{6}t} - e^{-4.76x10^{8}t})\ kV/m\ . \qquad (3.1)$$

Standard plane wave reflection coefficients were used to obtain the total field at the earth's surface, which is shown in Figure 3.2 for the two values of conductivity used in the study. The cables studied were shorted on one end and open on the other.

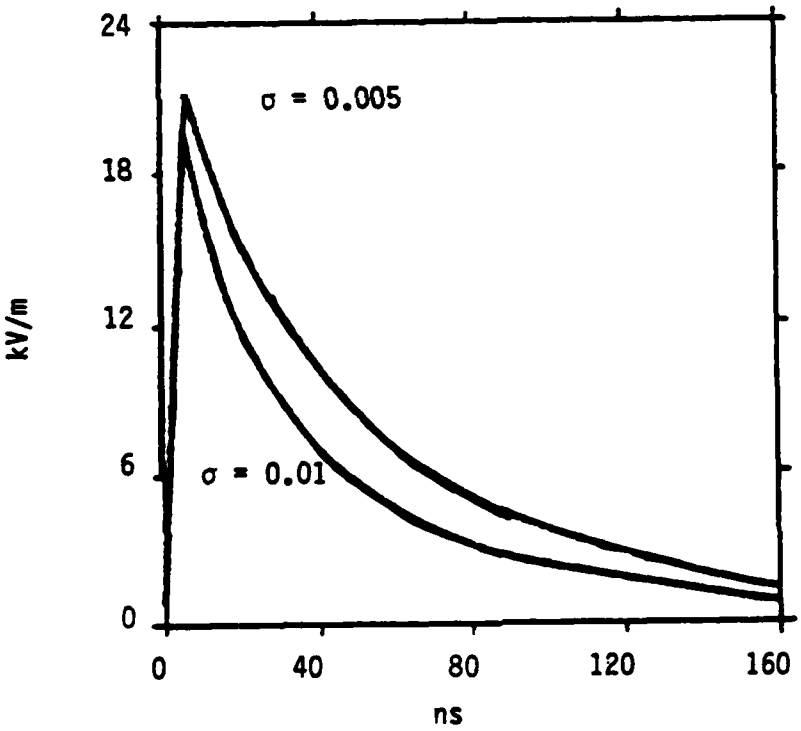

Figure 3.2 Total HAB Electric Field at Earth's Surface

HAB results are summarized in Figures 3.3 through 3.8. Some general remarks can be made about the HAB results. First, it was found that the results for lengths 100 m or greater were independent of length, within 1%. That is, the spectral content of the HAB input is of sufficiently high frequency so that signals propagating from one end toward the other attenuate rapidly and are not discernible at the far end. This is evident in Figure 3.3 which shows the short circuit current. The response from the other end should be arriving at about 700-800 ns assuming a nominal propagation velocity of one-half that of light, and it is clear that no such signal is there.

The second observation is that the voltage induced on the RG 8 dielectric is insufficient to cause breakdown (52 kV is required), and RG 58 breaks down only for the case σ = .005 mho/m.

From Figure 3.3 it is evident that the nonlinearities (both soil and dielectric) do not make a significant difference in the short circuit current response. For this case, only the three cells closest to the open end broke down, and this effect is not felt at the shorted end nearly 100 m away. The three cells closest to the open end broke down at 267, 172, and 270 ns, ordered in the direction from the shorted end to the open end, respectively.

It is also evident that the soil nonlinearities (which occur even if the dielectric does not break down) are unimportant in the current response as evidenced in Figures 3.3 and 3.6. It also makes little difference in the soil and dielectric voltages as evidenced in the RG 8 responses of Figures 3.7 and 3.8, which show essentially the same response for linear and soil nonlinear cases.

For the case in which the RG 58 dielectric breaks down, the voltages across the soil and dielectric are quite different from the linear case as one would expect, and this difference is evidenced in Figures 3.4 and 3.5. It is noted the end of the cable was artificially forced to be open, which is why the dielectric voltage of Figure 3.5 does not go to zero.

Finally, it is noted that the voltages induced on the cable are sufficient to cause air breakdown, which was not included in the model. For RG 58 from Figure 3.5 and Table 3.3, one gets an electric field in the air above the cable more than 7 MV/m, which is sufficient to cause air breakdown. For RG 8, the field is larger than 3.6 MV/m, which is still more than enough.

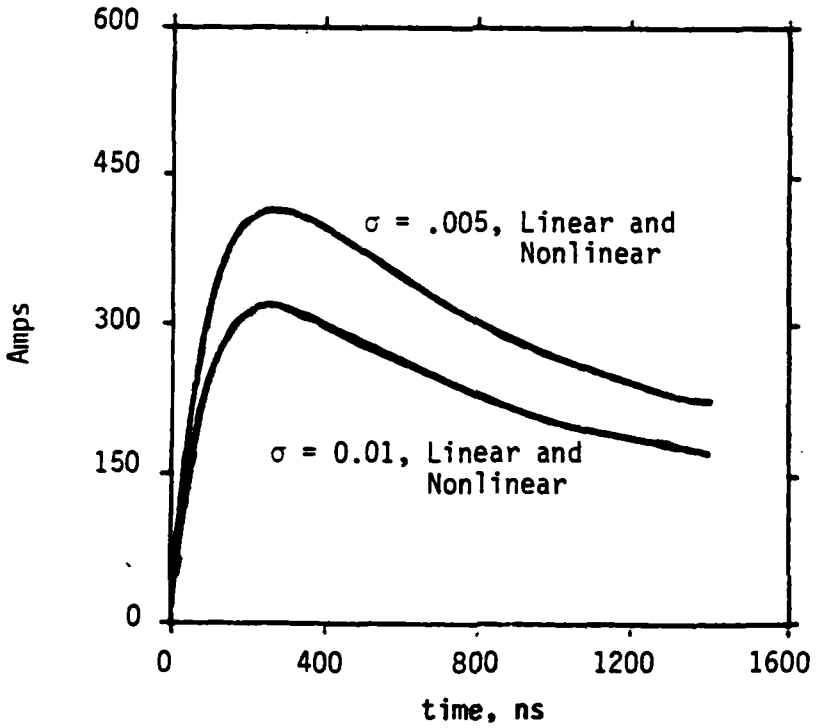

Figure 3.3 HAB Short Circuit Current on 100 m RG 58 Cable.

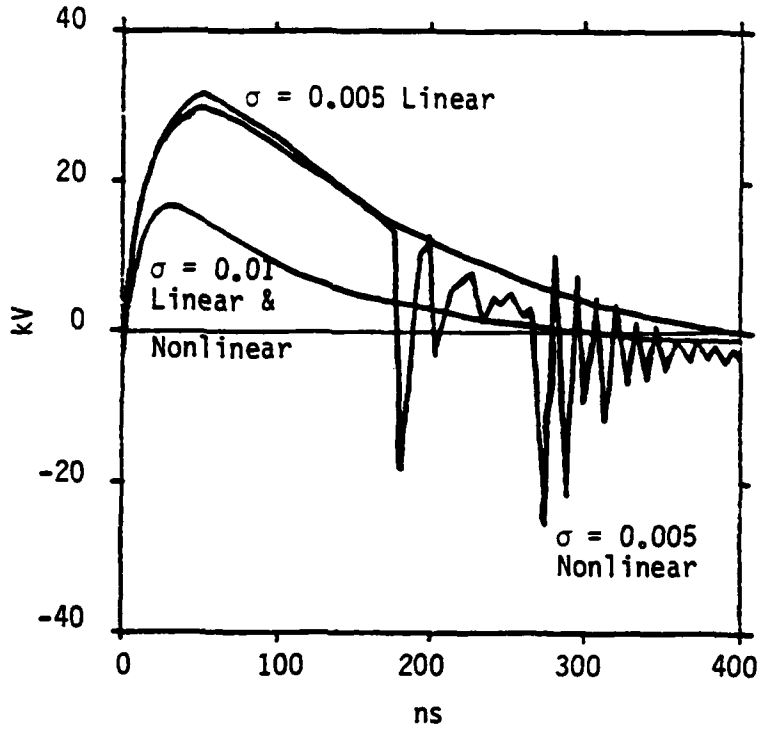

Figure 3.4 HAB Soil Voltage on Open End for 100 m RG 58 Cable.

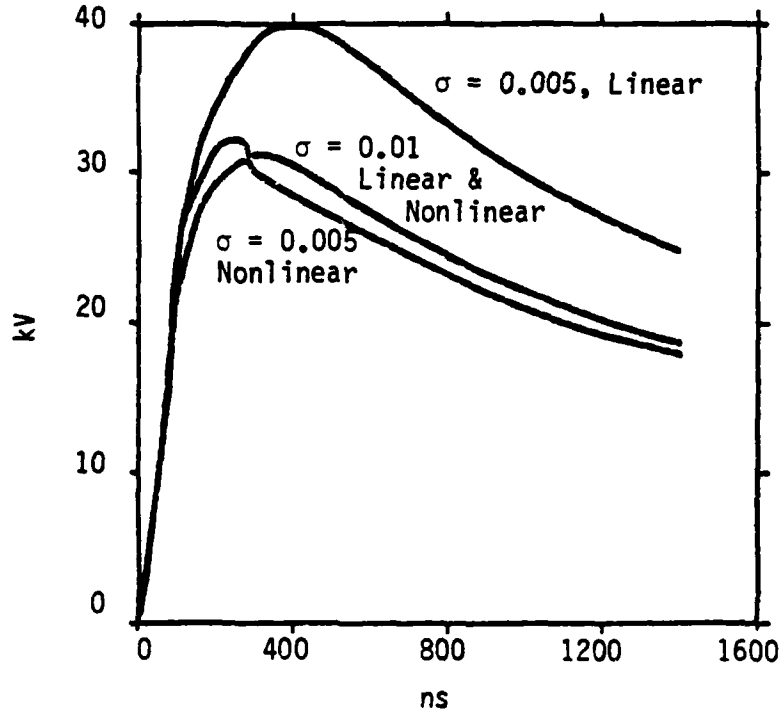

Figure 3.5 HAB Dielectric Voltage on Open End for 100 m RG 58 Cable.

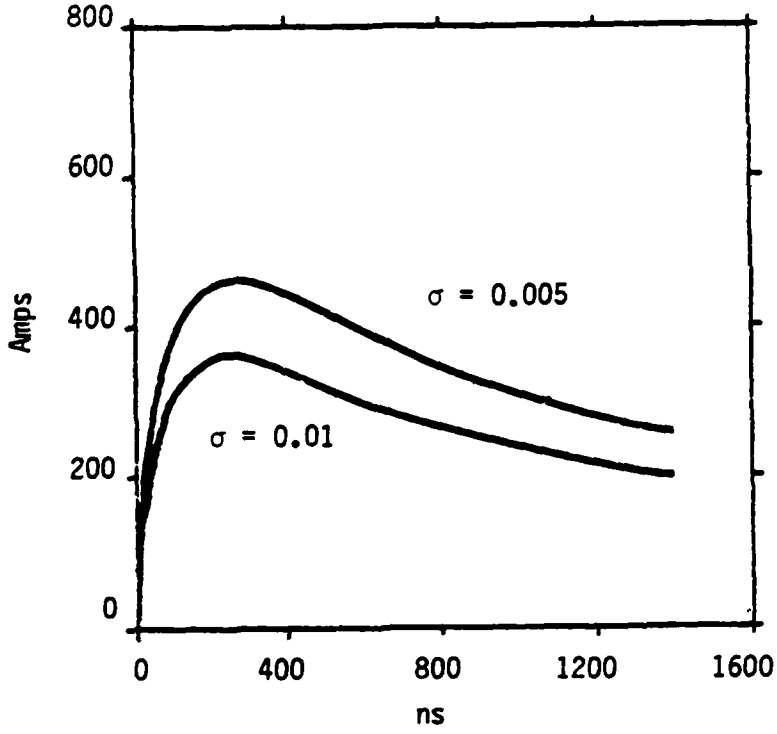

Figure 3.6 HAB Short Circuit Current for 100 m RG 8 Cable. Linear and Nonlinear.

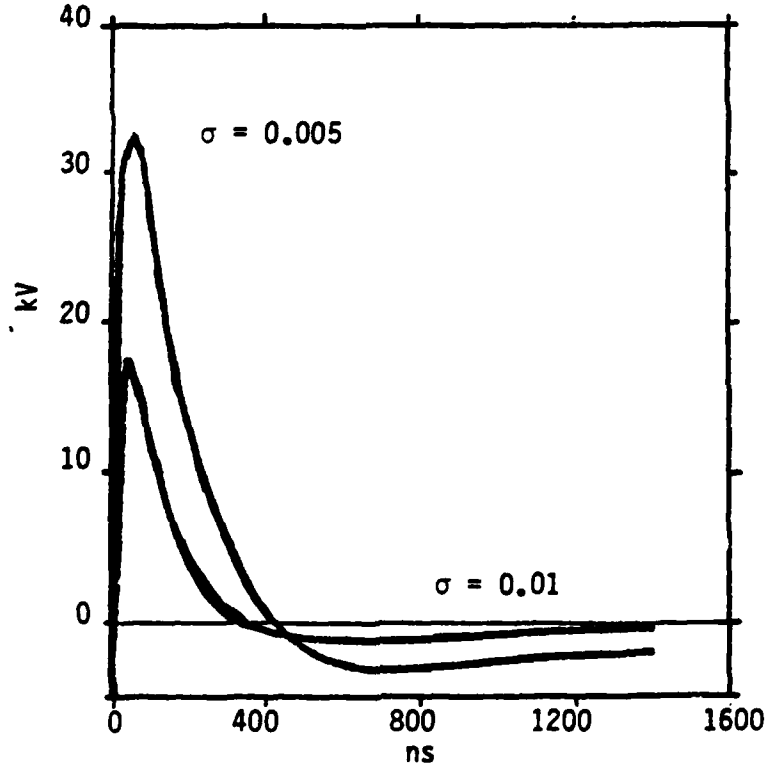

Figure 3.7 HAB Soil Voltage on Open End of 100 m RG 8. Linear and Nonlinear.

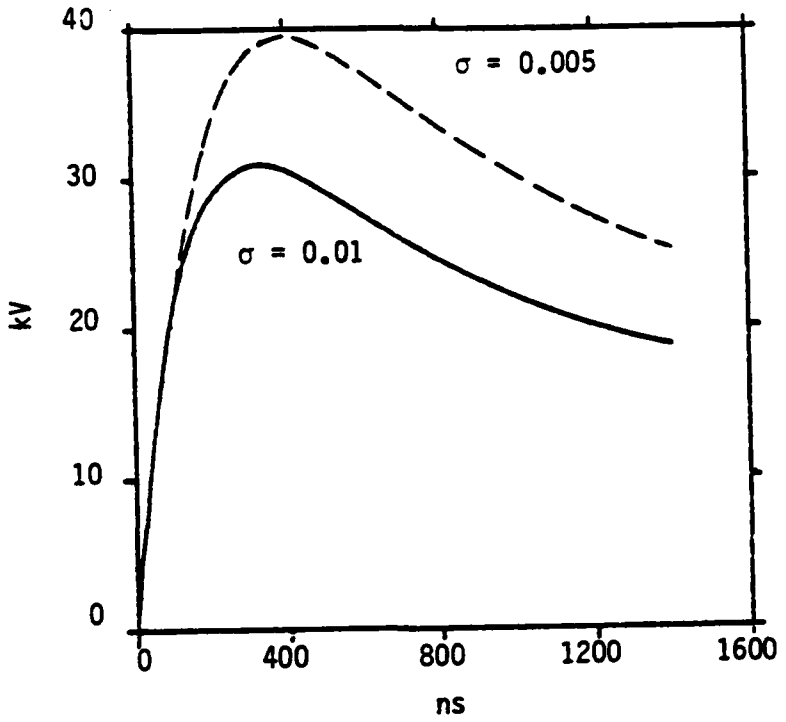

Figure 3.8 HAB Dielectric Voltage on Open End of 100 m RG 8. Linear and Nonlinear.

3.3 Computations for a Tactical Environment

The tactical environment which excites and influences the cable response is the radial electric field and the air conductivity. HDL supplied waveforms for these variables at ranges from 50 to 2800 meters which were used in the computations. Typical waveforms are shown in Figures 3.9 and 3.10 which are for a range of 1000 m. Cables of 100, 600, and 2800 m length were studied. In all cases, they are oriented radially to the source, and the end closest to the source is a perfect short and the end farthest away from the source is open circuited (except for one 2800 m case, discussed later). Responses computed are the short circuit current at the shorted end, and the dielectric voltage and soil voltage at the open end.

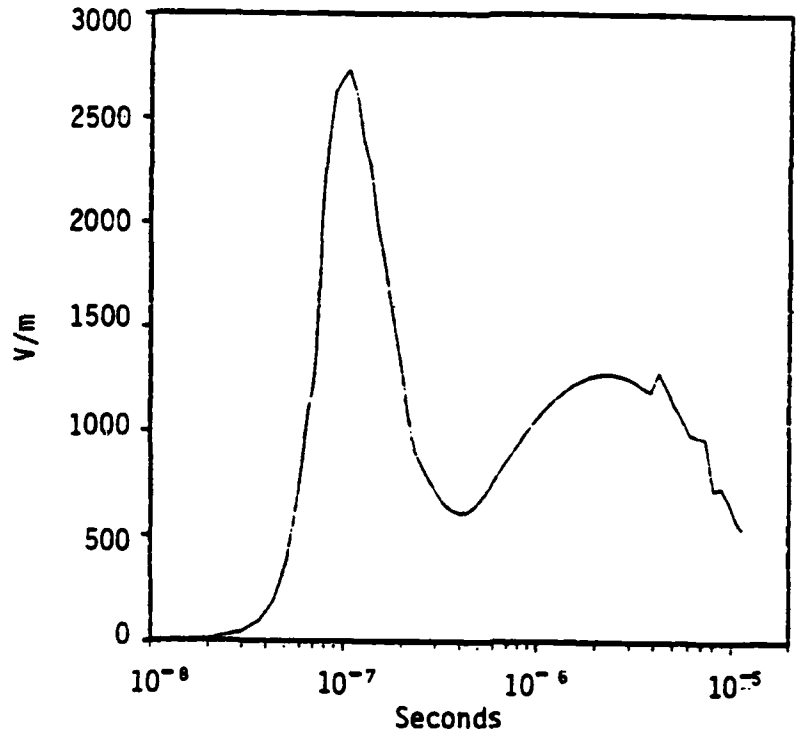

Figure 3.9 Tactical Radial Electric Field at 1000 m Range.

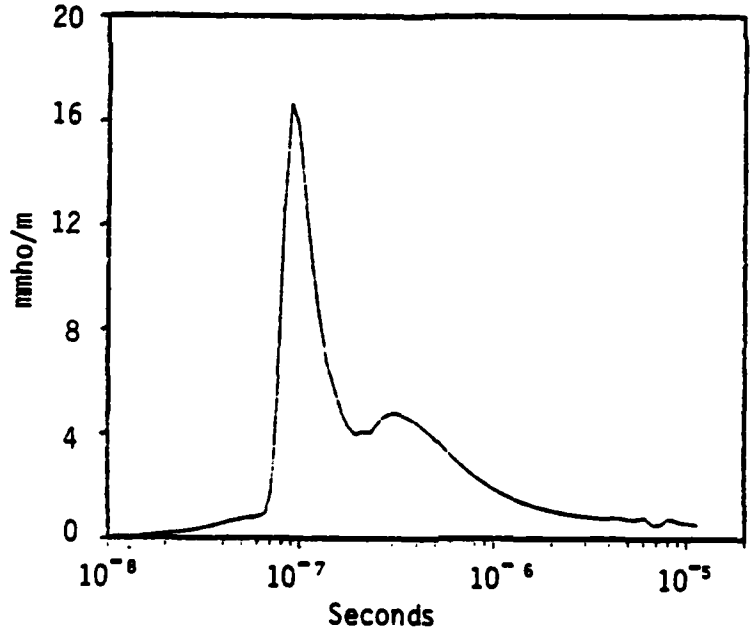

Figure 3.10 Tactical Air Conductivity at 1000 m Range.

Results for the 100 m cable are shown in Figures 3.11 through 3.16. The cable is located between the ranges of 900 and 1000 m. The effect of the nonlinearities is to greatly increase the short circuit current, as shown in Figures 3.11 and 3.12. The late time response is also greatly extended. The effect of nonlinearities on the soil voltage is to reduce it and significantly alter the spectral content as evidenced in Figures 3.13 and 3.14. Of course, as one would expect, the effect of the nonlinearity is to greatly decrease the dielectric voltage.

The propagation of dielectric breakdowns for the 100 m cable is interesting. For example, for the RG 58 at σ = .005, the dielectric breakdowns begin at the open end at t = 1.63 μsec and propagate a distance of 38.7 meters toward the source, at which point breakdown occurs at 7.95 μsec. It appears likely that if the computation were extended in time, the punctures would propagate even further.

Results for the 600 m cables are shown in Figures 3.17 through 3.22. One end is at a range of 400 m and the other is at 1000 m. Results are similar in character to those of the 100 m cables except that the responses are much larger. The propagation of dielectric breakdowns is more complex in this case than for the 100 m case. For RG 58 at σ = .005, the first puncture occurs at 92 meters from the shorted end at 3.23 μsec and propagates both directions; inward to 74 meters at 3.3 μsec, and then outward every 6.6 meters (approximately). In addition, breakdown occurs at the far end at 3.37 μsec and propagates inward a distance of 66 meters where breakdown occurs at 12.6 μsec. The end result is a complex pattern of punctures which is non-uniformly distributed along the cable. There are no punctures at distances closer than 74 meters to the source end of the cable.

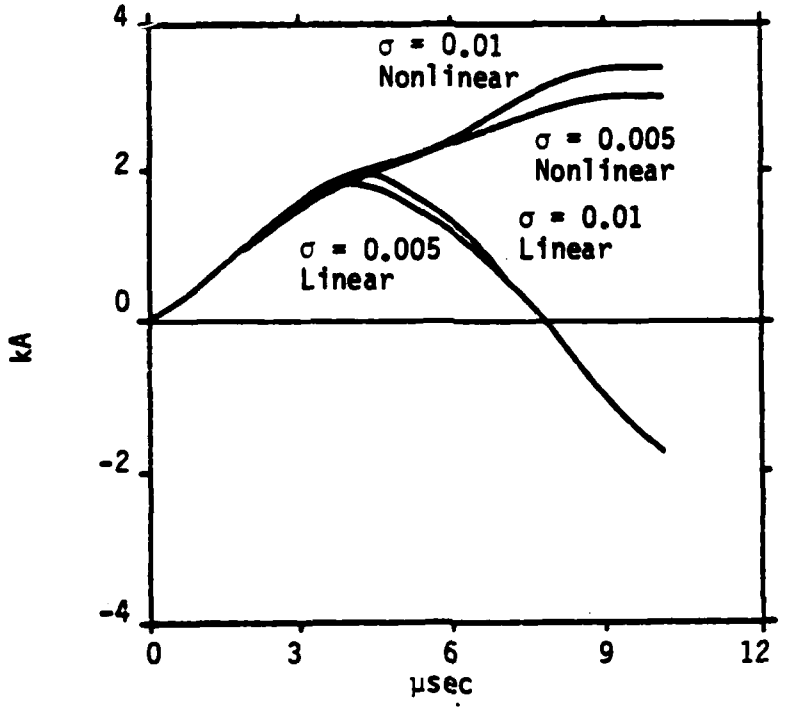

Figure 3.11 Tactical Short Circuit Current for 100 m RG 58 Cable.

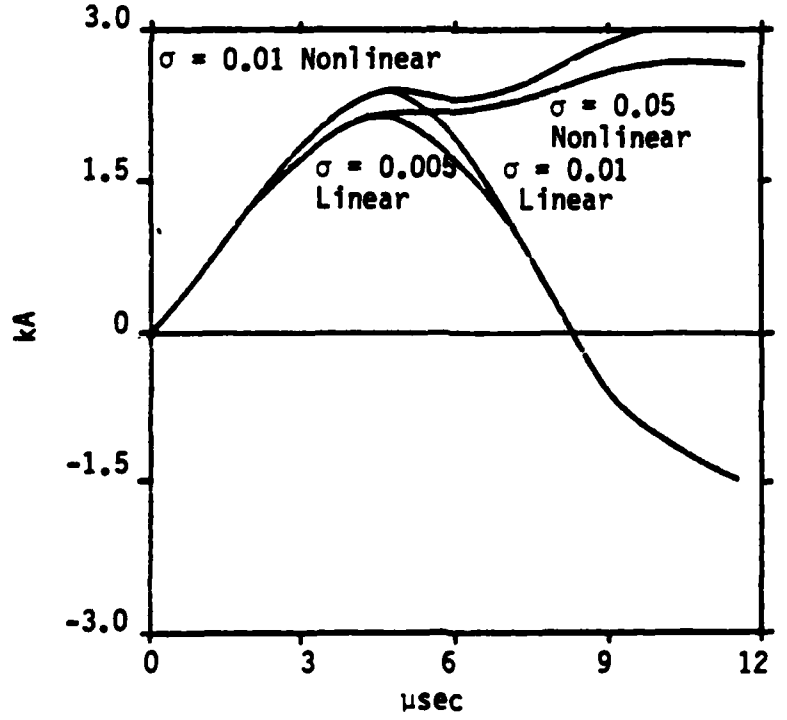

Figure 3.12 Tactical Short Circuit Current for 100 m RG 8 Cable.

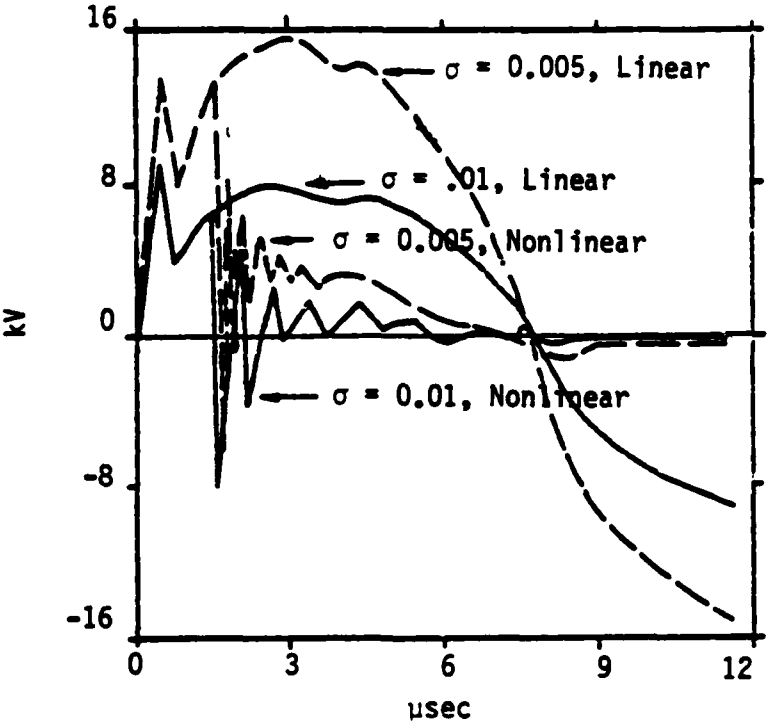

Figure 3.13 Tactical Soil Voltage for 100 m RG 58 Cable.

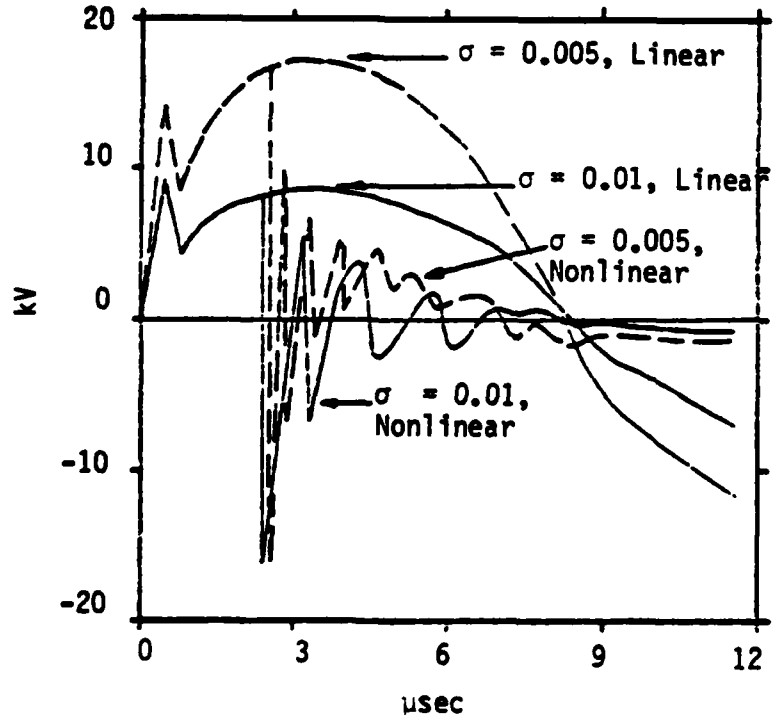

Figure 3.14 Tactical Soil Voltage for 100 m RG 8 Cable.

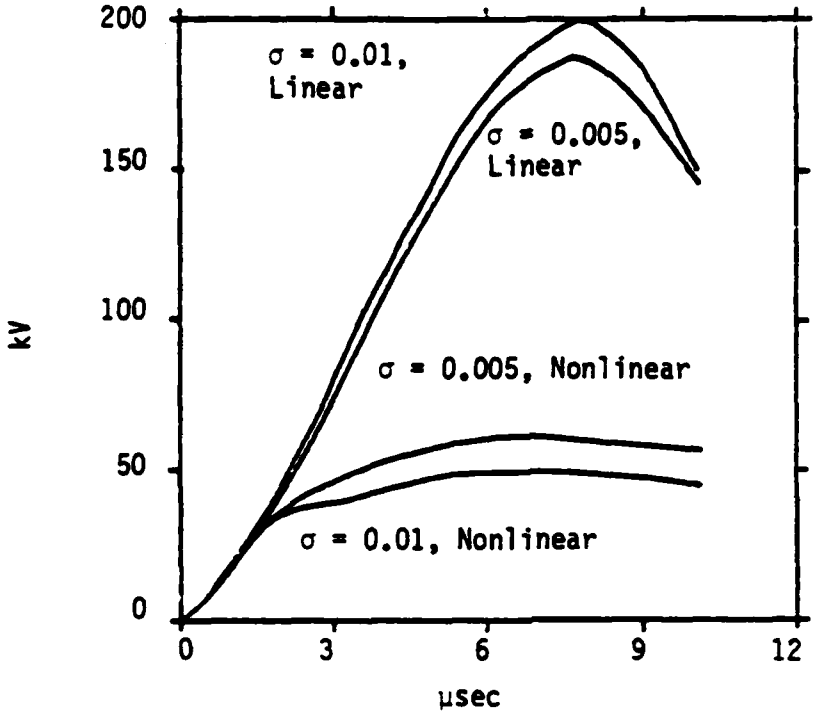

Figure 3.15 Tactical Dielectric Voltage for 100 m RG 58 Cable.

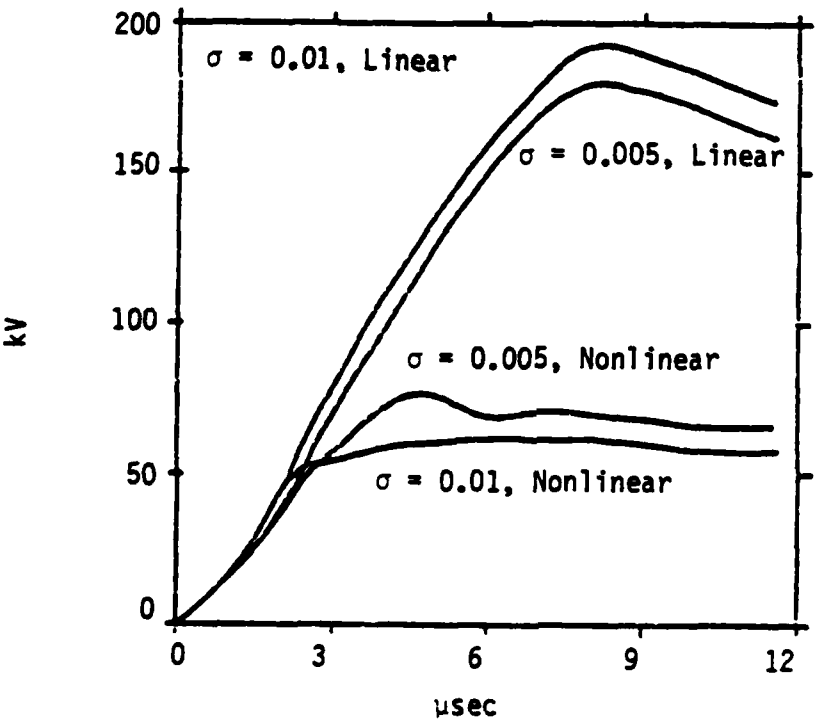

Figure 3.16 Tactical Dielectric Voltage for 100 m RG 8 Cable.

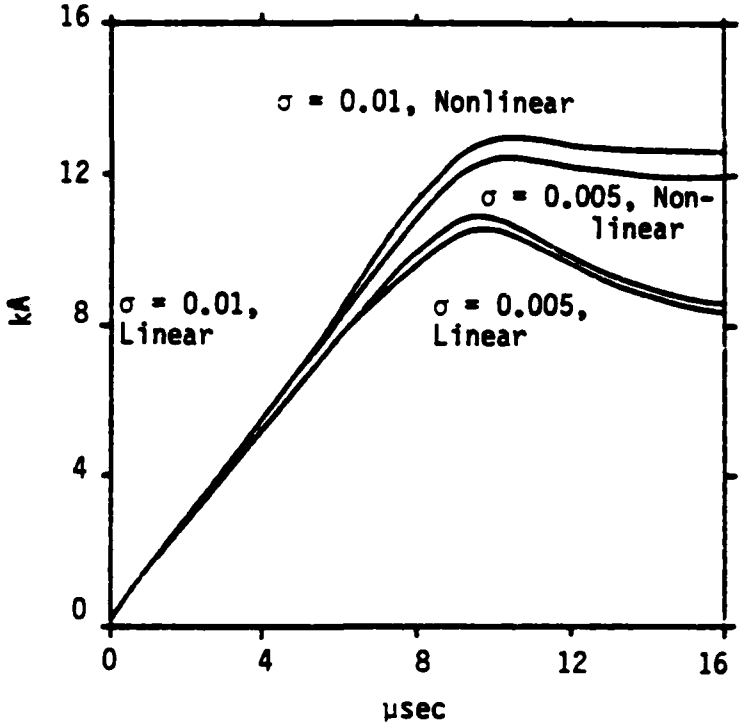

Figure 3.17 Tactical Short Circuit Current for 600 m RG 58.

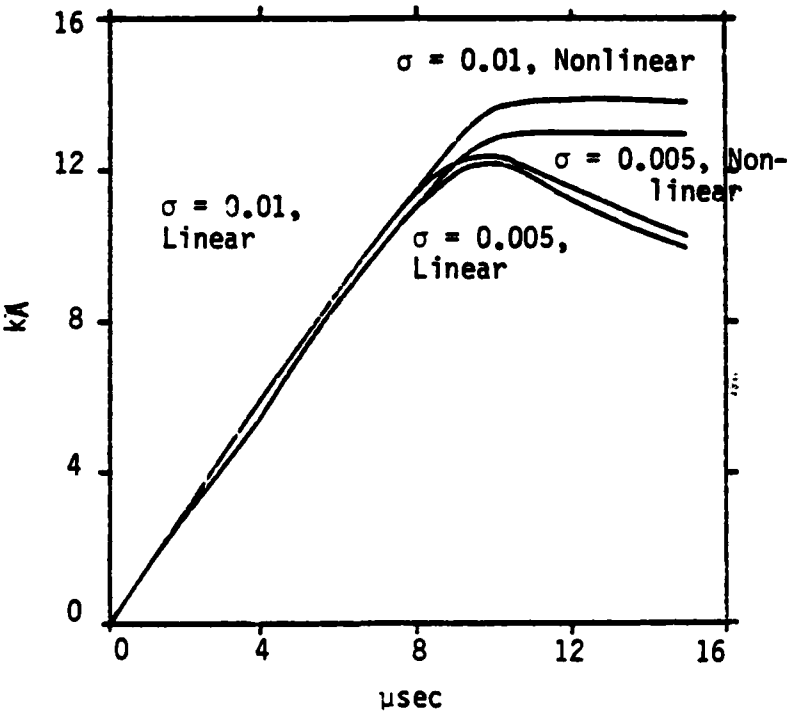

Figure 3.18 Tactical Short Circuit Current for 600 m RG 8.

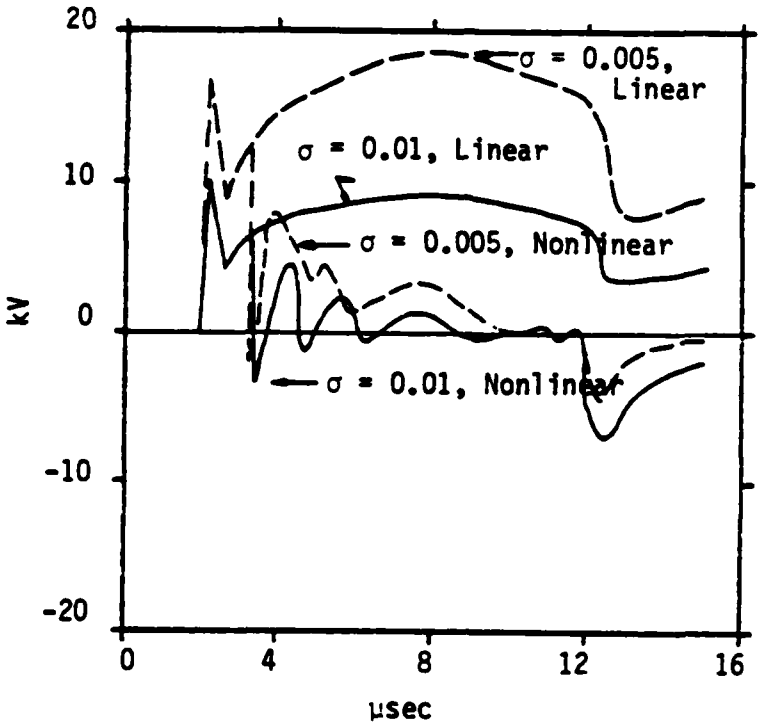

Figure 3.19 Tactical Soil Voltage for 600 m RG 58.

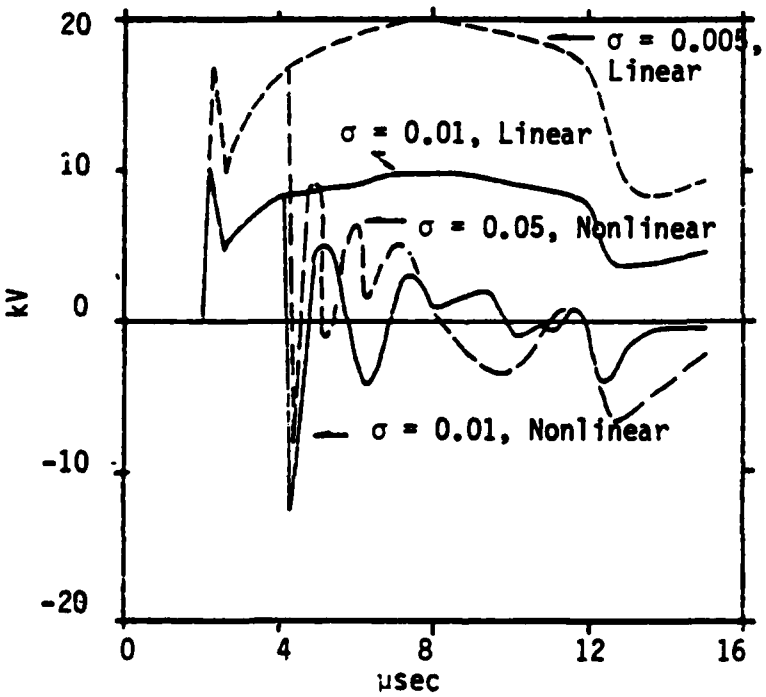

Figure 3.20 Tactical Soil Voltage for 600 m RG 8.

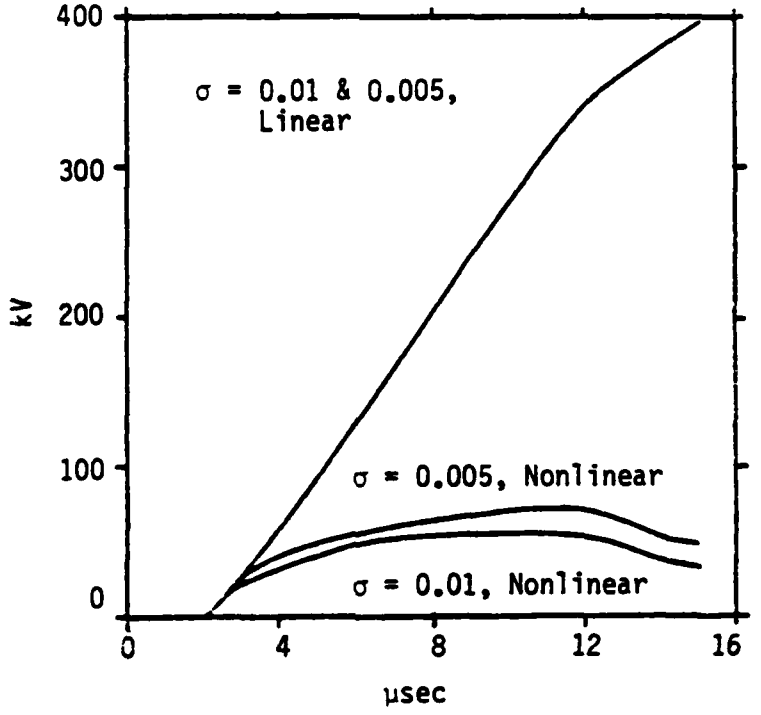

Figure 3.21 Tactical Dielectric Voltage for 600 m RG 58.

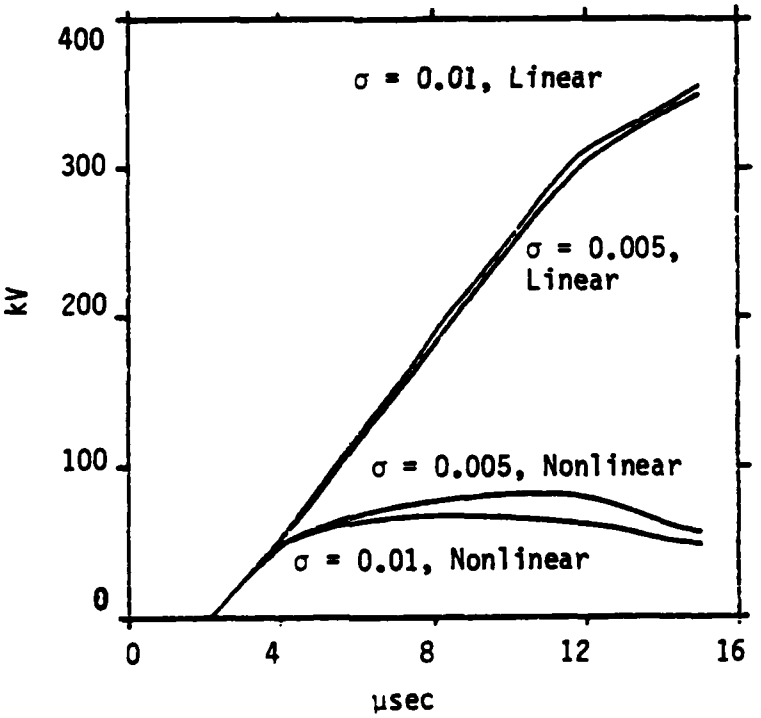

Figure 3.22 Tactical Dielectric Voltage for 600 m RG 8.

Results for the 2800 m cable are given in Figures 3.23 through 3.28. Cable currents are similar in character and in amplitude to those for the 600 m cable. The effect of the nonlinearities is to greatly increase the late time response. Also, the nonlinearities greatly reduce the dielectric voltages and significantly alter the amplitude and wave-shape of the soil voltages.

The pattern of dielectric punctures is quite complex for this case also. For the RG 58 with σ = .005, the first puncture occurs at 280 m at 3.18 μsec. The puncture closest to the source is at 60 m and occurs at 3.3 μsec. The far end breaks down at 13.8 μsec, but this is the only puncture in the last 500 meters of the cable. The remainder of the cable has a complex distribution of punctures.

For all of the tactical computations, voltage levels are higher than those obtained for the HAB case. Thus it is clear that the air will break down also, an effect not included in these computations but which should be considered in the future.

Because there is some interest in knowing what the short circuit current at the far end of the 2800 m cable is, it was also calculated (with both ends shorted) and is shown in Figure 3.29. It is noted that the linear and nonlinear cases agree. This is because there is no dielectric breakdown in the last 500 meters of the cable, and the effects of breakdown are not significant by the time they propagate to the far end.

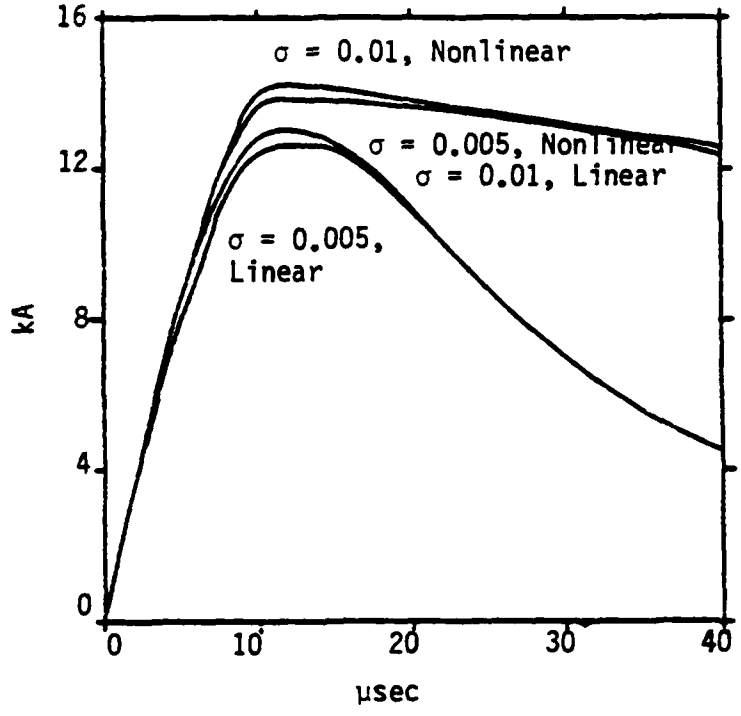

Figure 3.23 Tactical Short Circuit Current for 2800 m RG 58 Cable.

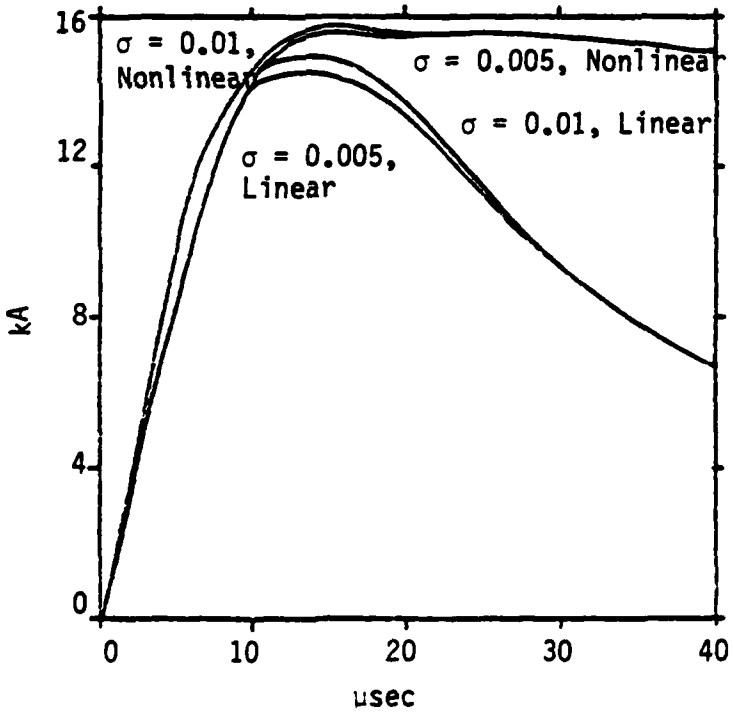

Figure 3.24 Tactical Short Circuit Current for 2800 m RG 8 Cable.

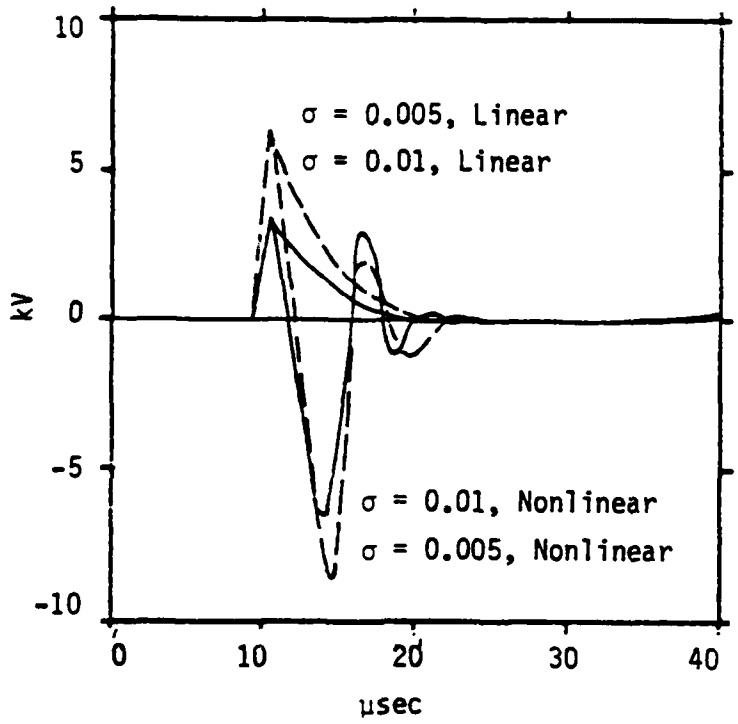

Figure 3.25 Tactical Soil Voltage for 2800 m RG 58 Cable.

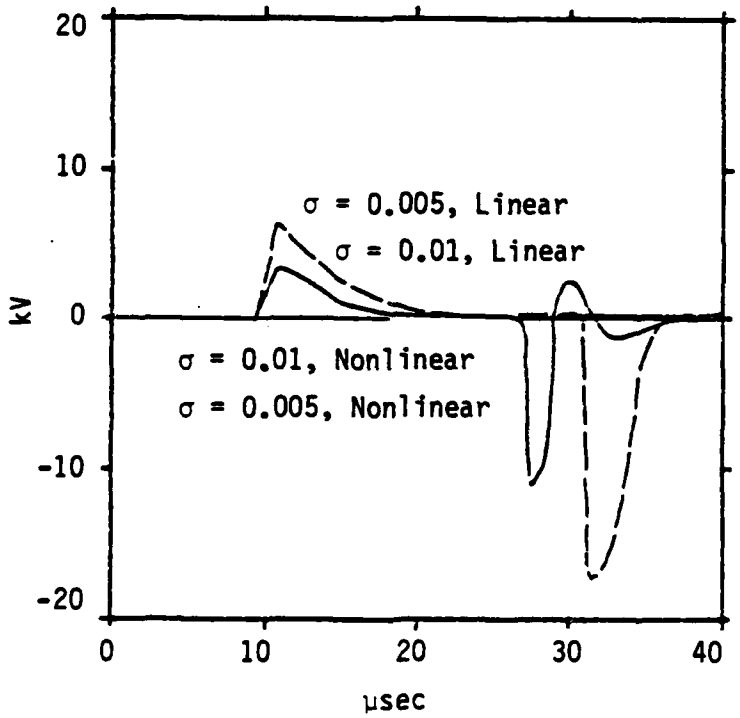

Figure 3.26 Tactical Soil Voltage for 2800 m RG 8 Cable.

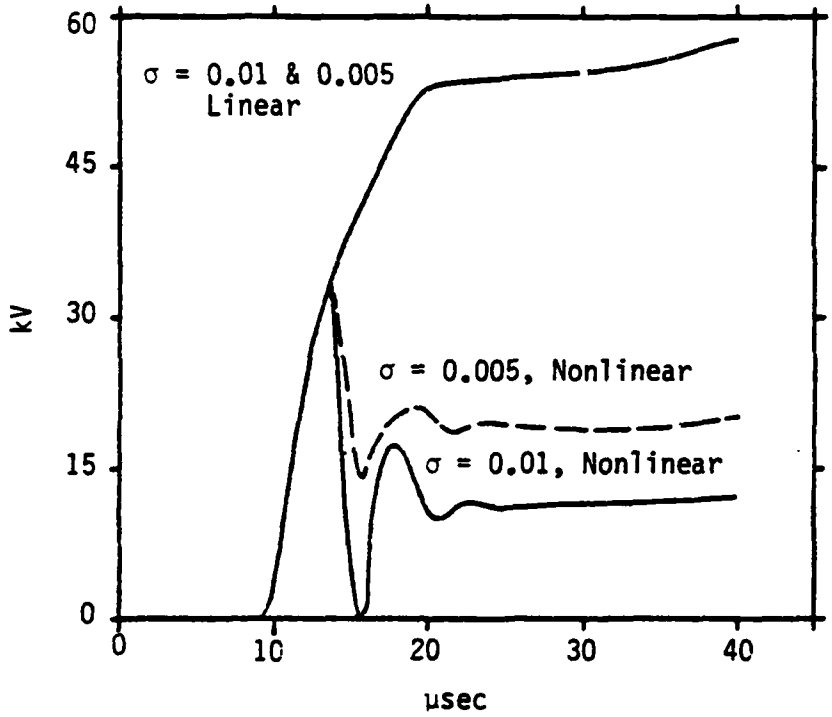

Figure 3.27 Tactical Dielectric Voltage for 2800 m RG 58 Cable.

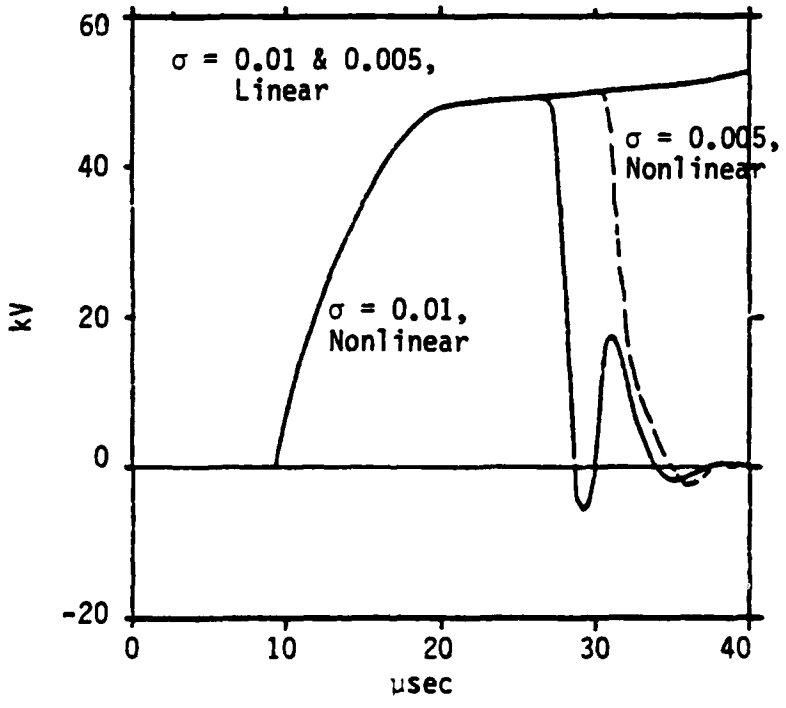

Figure 3.28 Tactical Dielectric Voltage for 2800 m RG 8 Cable.

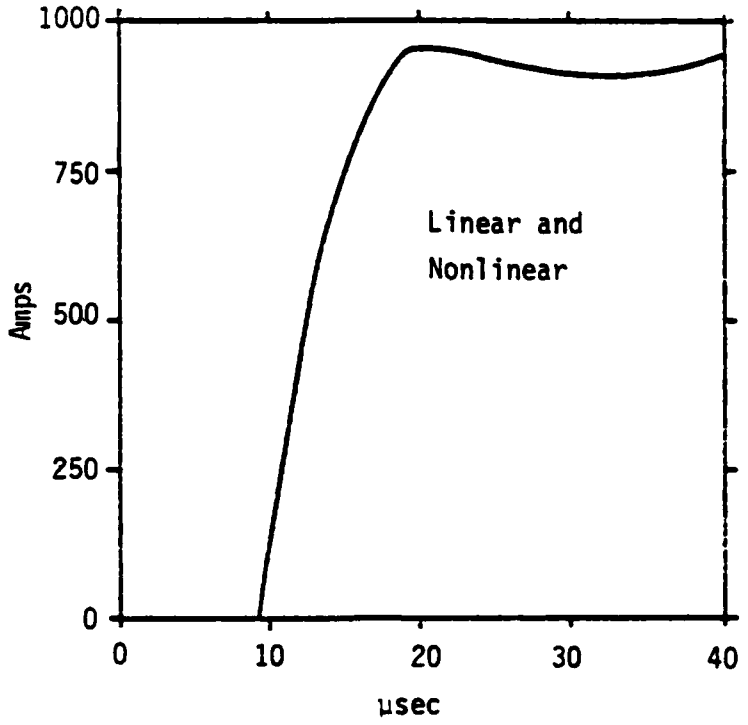

Figure 3.29 Short Circuit Current at the Far End of the 2800 m RG 58 Cable. Ground Conductivity is .01 mho/m.

SECTION 4

EXPERIMENT FEASIBILITY

4.1 Background

One of the goals of this study was to determine the feasibility of using existing simulators to investigate nonlinear cable response. Computations were done using AESOP, which has the same electromagnetic characteristics as TEMPS, as the source of EMP fields to illumine the cables into their nonlinear response regimes. It was found that AESOP can indeed be used to perform these experiments. In order to do this study, the electromagnetic field model of AESOP had to be determined. Then some experimental concepts are given, and then some computational results are shown.

For the purposes of this section, three cable responses were computed, both with and without nonlinear effects included. Figure 4.1 illustrates the type of cable configurations that were studied. A small coaxial cable like RG 58 would make a reasonable test cable for the insulated cable and 1/2" electrical conduit would suffice for the uninsulated conduit.

The three experiments include most of the interesting effects. The U-shaped insulated cable will exhibit a voltage maximum at the base of the U. If breakdown occurs, it will begin in the U-shaped region. Several punctures of the dielectric are likely to occur. The principal question is at what minimum field intensity will a puncture of the insulating jacket be obtained. Additionally, one would like to know the periodicity of breakdowns along the cable in the case where a very high field intensity pulse is applied to an undamaged cable.

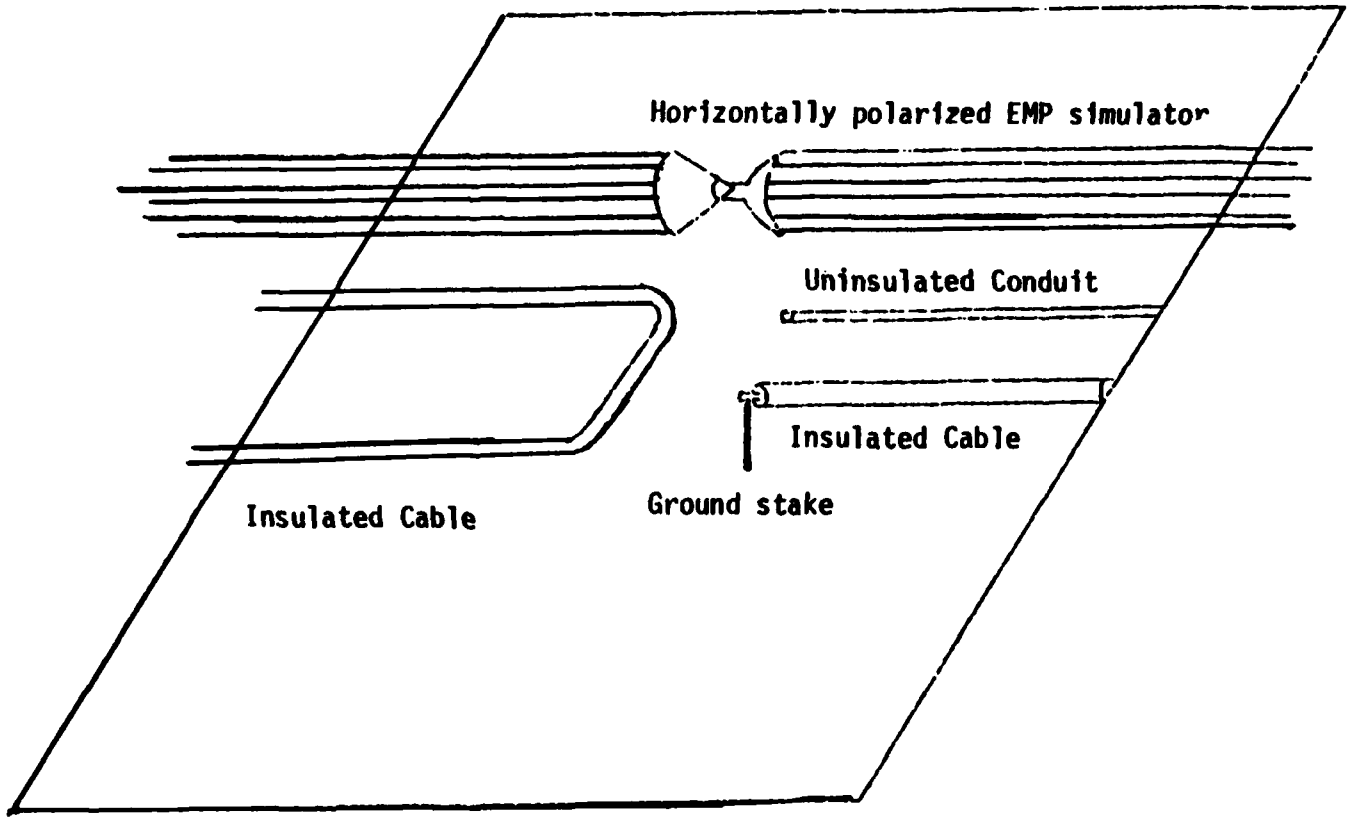

Figure 4.1 Cable Dielectric Breakdown and Soil Nonlinearity Experiments for Surface Cable Studies.

The uninsulated conduit will be a test of our understanding of the nonlinear response of soil, unconfused by the mixing of dielectric breakdown and soil breakdown.

The ground stake experiment will examine the ground stake response as a termination impedance. This tests directly the model of nonlinear incremental soil parameters without including distributed parameters and distributed sources in the analysis.

4.2 The AESOP Field Model

The model used to predict the fields is the same as that of Reference 19. The electromagnetic fields produced by AESOP are much more complicated than the high altitude burst plane waves. For AESOP, the amplitude, angle of incidence, and the wave polarization are a function of position, whereas they are not for HAB.

Figure 4.2 shows an oblique view of AESOP and the coordinate system. The antenna is on the z axis at $y = x = 0$. It is 20 meters above the earth. If one draws a vector from the origin at (0, 0, 0) to another point (x, y, z) where the fields are to be defined, it is useful to define the angles β and ϕ according to the following:

$$\cos \beta = \frac{z}{\sqrt{x^2 + y^2 + z^2}}$$

$$\cos \phi = \frac{y}{\sqrt{x^2 + y^2}} \qquad (4.1)$$

The radiated fields are found from the formulas of Jordon [20] for fields near a dipole and are expanded in a power series to obtain the fields before reflection from the ends take place. This is equivalent to making the antenna infinitely long, or else having a long antenna with perfectly matched terminations on each end.

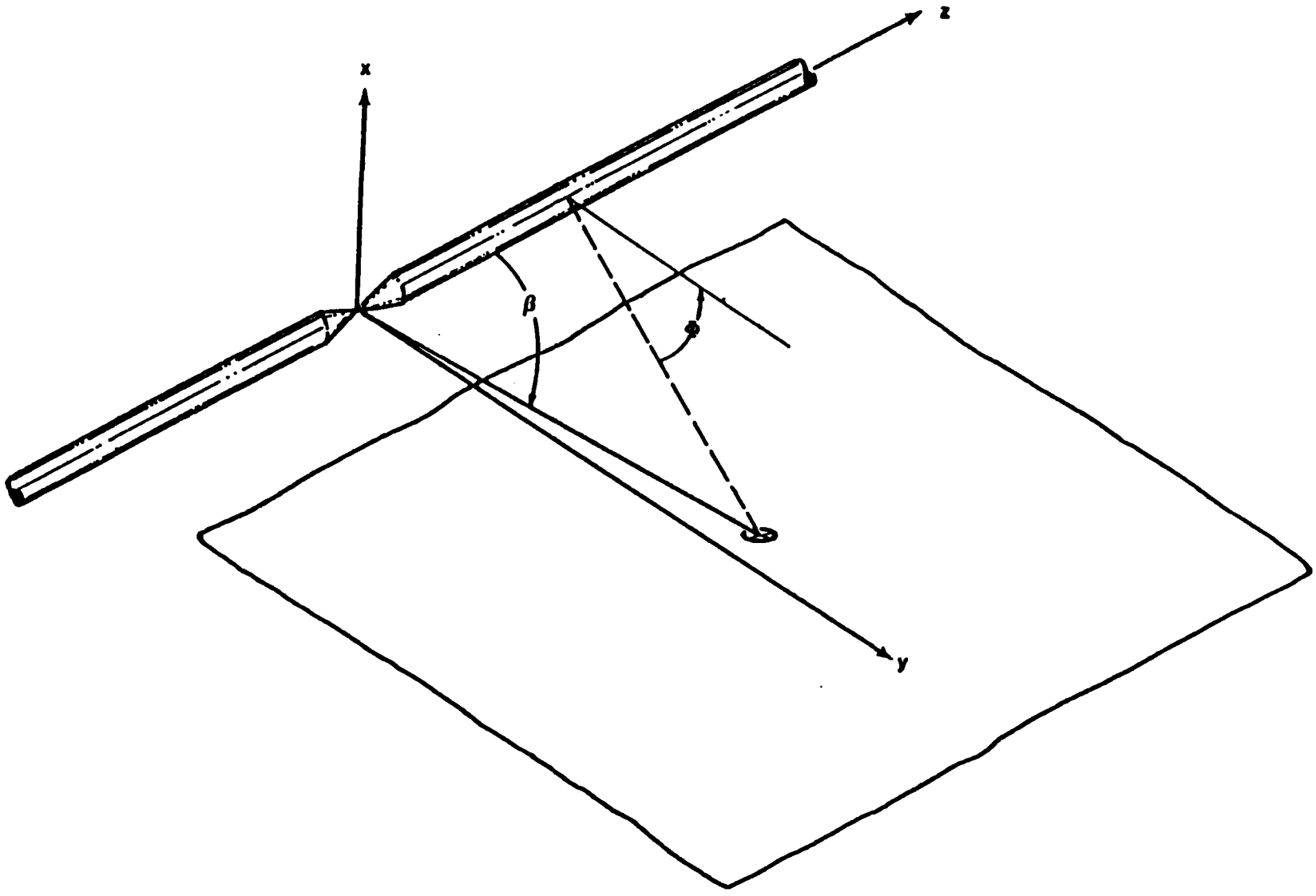

Figure 4.2 Three-Dimensional View of AESOP with Coordinate System.

The resultant total electric and magnetic fields are

$$E_t = \frac{V_o}{\psi \sqrt{x^2 + y^2}}$$

and

$$H_\phi = \frac{-E_t}{Z_o} \tag{4.2}$$

where V_o is the pulser voltage and ψ is a constant, and are chosen to normalize the incident electric field to 50 kV/m at the earth at the coordinate y = 50 m. The field and its spectral content are shown in Figure 4.3 and 4.4, respectively.

The unit vector $\hat{U}_p$ perpendicular to the plane of incidence is given by

$$\hat{U}_p = \frac{1}{\sqrt{\sin^2\beta \cos^2\phi + \cos^2\beta}} \left[\hat{U}_z (\sin\beta \cos\phi) - \hat{U}_y (\cos\beta) \right. \tag{4.3}$$

Then the incident horizontally polarized and vertically polarized incident fields are given by

$$\left.\begin{aligned} \bar{E}_{HP_{INC}} &= \frac{E_t \cos\phi}{(\sin^2\beta \cos^2\phi + \cos^2\beta)^{1/2}} \hat{U}_p \\ \bar{H}_{VP_{INC}} &= \frac{-E_t}{\eta_o} \frac{\sin\phi \cos\beta}{(\sin^2\beta \cos^2\phi + \cos^2\beta)^{1/2}} \hat{U}_p \end{aligned}\right\} \tag{4.4}$$

An approximation is made that the plane wave reflection coefficients [21] for the earth can be used. The total field parallel to the surface cables is then computed and used as the excitation source which drives them. The earth is assumed to have constitutive parameters $\varepsilon = 10\varepsilon_o$ and $\sigma = .005$ mho/m. The risetime of the AESOP field can be in the range of 4-12 ns., and a nominal value of 8 ns was used in the computations.

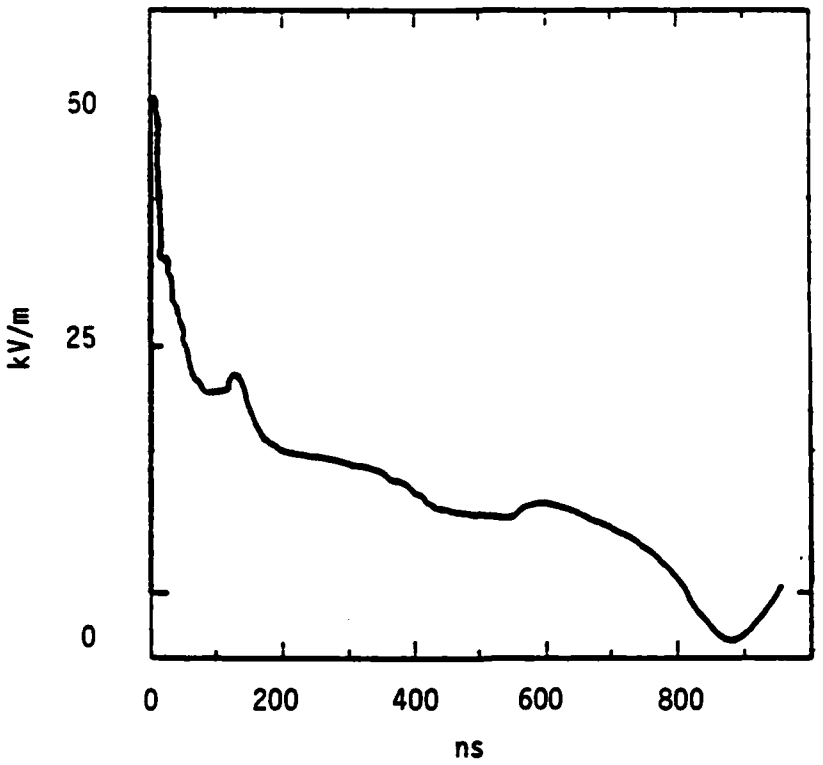

Figure 4.3 AESOP Incident Electric Field at (-20, 50, 0)

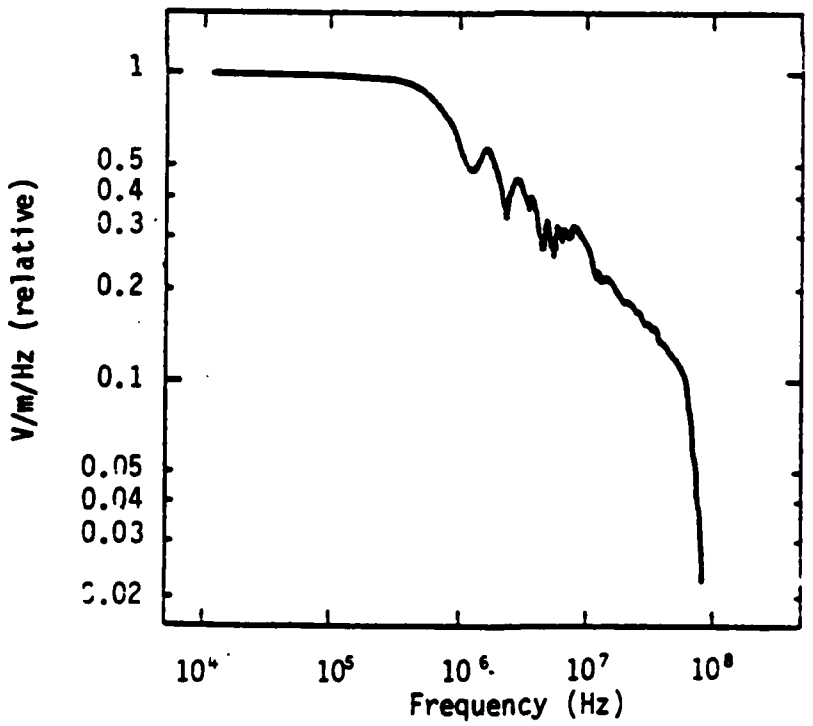

Figure 4.4 Spectral Content of AESOP Field

Figure 4.5 shows the total electric field at (-20, 3, 0). It was found that along a line from this point to (-20, 3, 37), the total electric field did not noticeably change waveshape and the peak amplitude decreased nearly linearly (within 3%) to a minimum of 45.2 kV/m. This line is the line upon which all of the cables to be studied were placed.

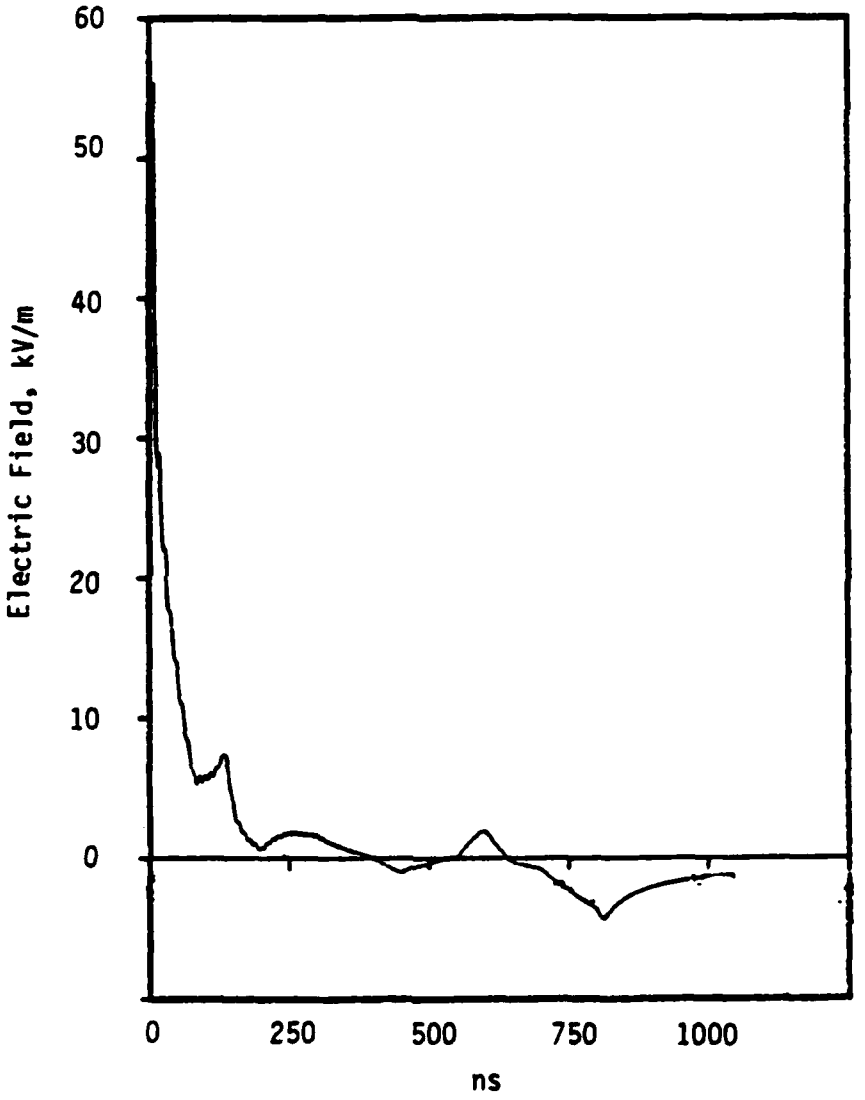

Figure 4.5 AESOP Total Electric Field at (-20, 3, 0).

4.3 Results for the Ground Stake Experiment

The ground stake experiment consisted of 37 meters of RG 58 with its shield terminated to a 1" OD ground stake of length 2 meters and the other end open circuited. The ground stake impedance is 98 Ω, according to the formulas of Sunde [10]. Figure 4.6 shows the stake current and Figure 4.7 shows the dielectric voltage at the other end of the cable for linear and nonlinear cases.

The current shows a small nonlinear effect, but it would be noticeable on a measurement. If one could measure the dielectric voltage, a marked difference could be observed.

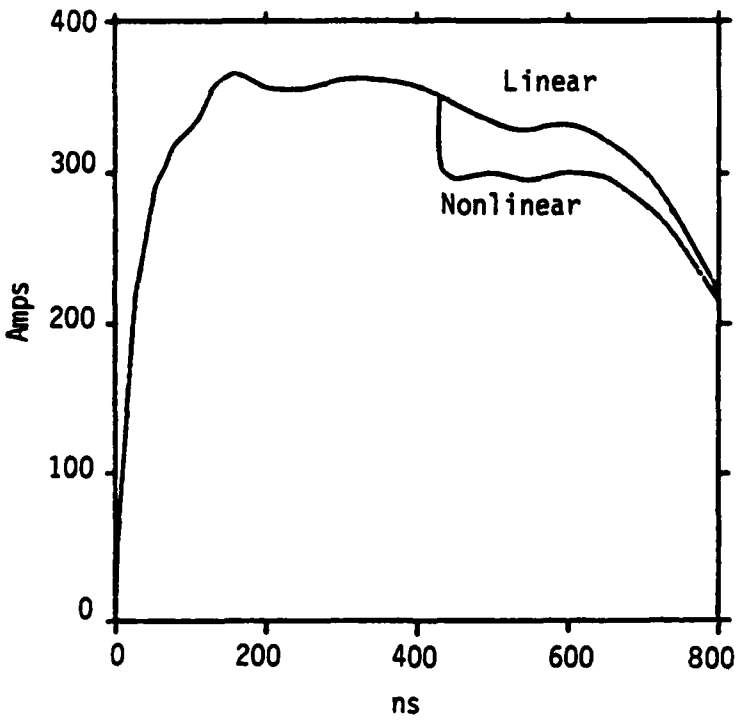

Figure 4.6 Stake Current.

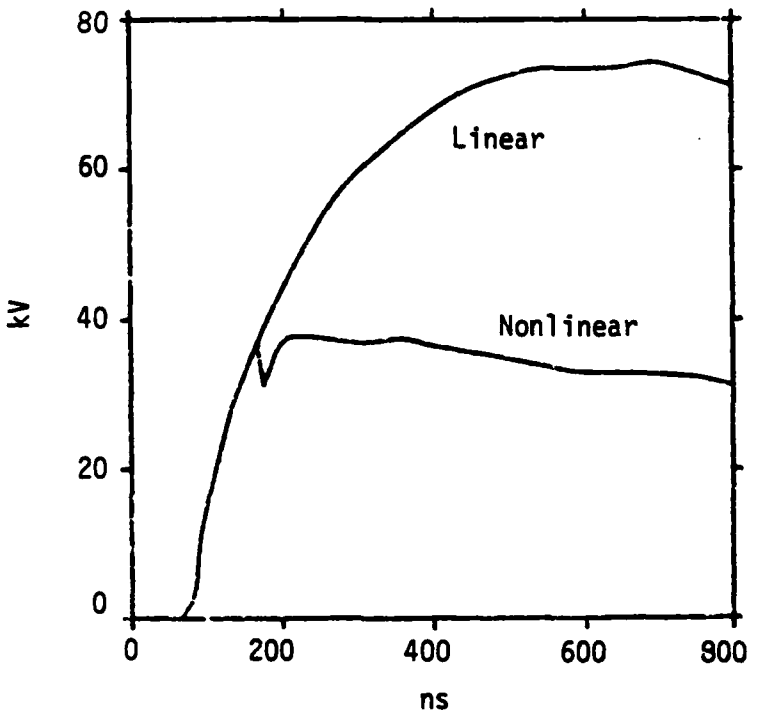

Figure 4.7 Dielectric Voltage at End of the Insulated Cable.

The computations indicate that the 7 meters of cable closest to the open end would experience multiple punctures. The first puncture occurs at the open end at 84 ns and the punctures propagate 7 meters and the last one occurs at 330 ns.

Because punctures occur only at the end away from the stake, their effect on the stake current is rather small. A shorter cable would probably cause a bigger difference in stake current, but even that in Figure 4.6 is discernible. From Figure 4.7, one may conclude that if one reduced the simulator output by a factor of 2, the nonlinearities would just be at the threshold of occurrence.

4.4 Bare Conduit Experiment

Figures 4.8 through 4.10 present the results for the 37 meter long bare conduit computations. These results are consistent with previous results in that only small effects in cable response are caused by soil nonlinearities. The results shown are computed from a much reduced value of bulk soil breakdown voltage: 375 kV/m. This was done because if one used 2 MV/m, the results nearly overlayed each other and it was desirous to ascertain the importance of the soil breakdown field. It appears that the non-sensitivity of response to soil breakdown above can be readily checked by this experiment.

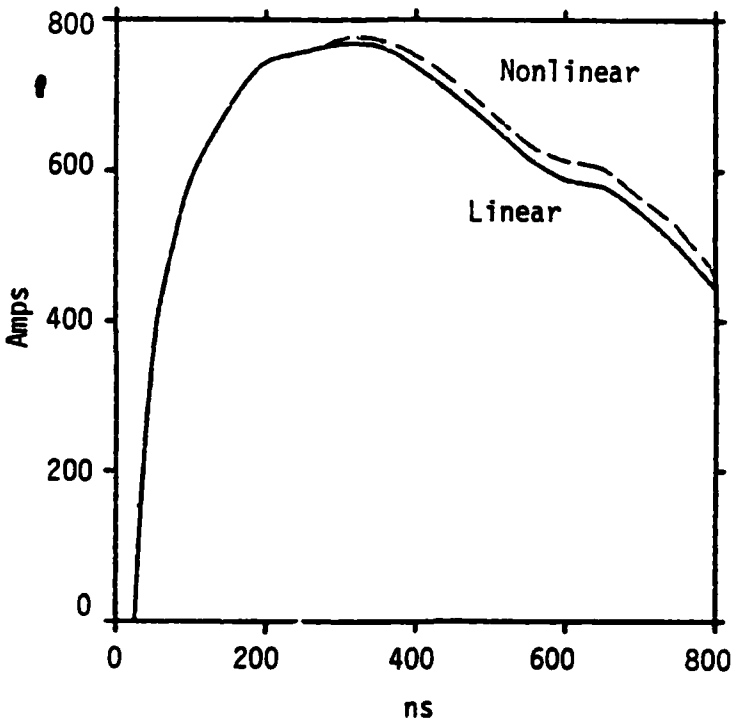

Figure 4.8 Conduit Center Current.

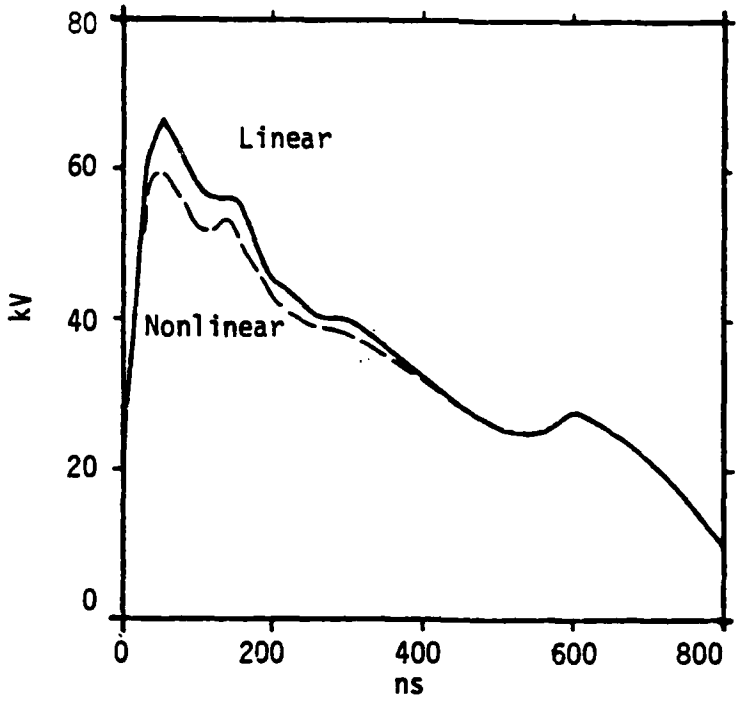

Figure 4.9 Voltage on Left End of Conduit.

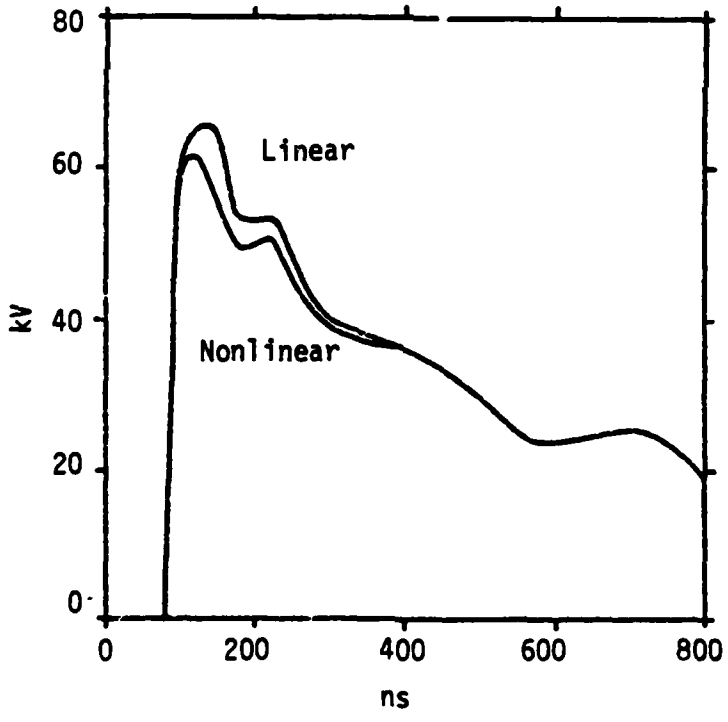

Figure 4.10 Voltage on Right End of Conduit.

4.5 "U" Cable Experiment

The "U" cable is 37 meters long on each side and the joining part is 6 meters long. The cable is open on the ends. Its response is predicted to show the most dramatic nonlinear effects. Results are presented in Figures 4.11 through 4.16.

The current response (Figures 4.11 through 4.13) should be easily measurable. The effect of the nonlinearities is to greatly increase the peak value and late time currents as shown. From the voltage waveforms, one can estimate that nonlinearities would begin to occur at about 50% of simulator output.

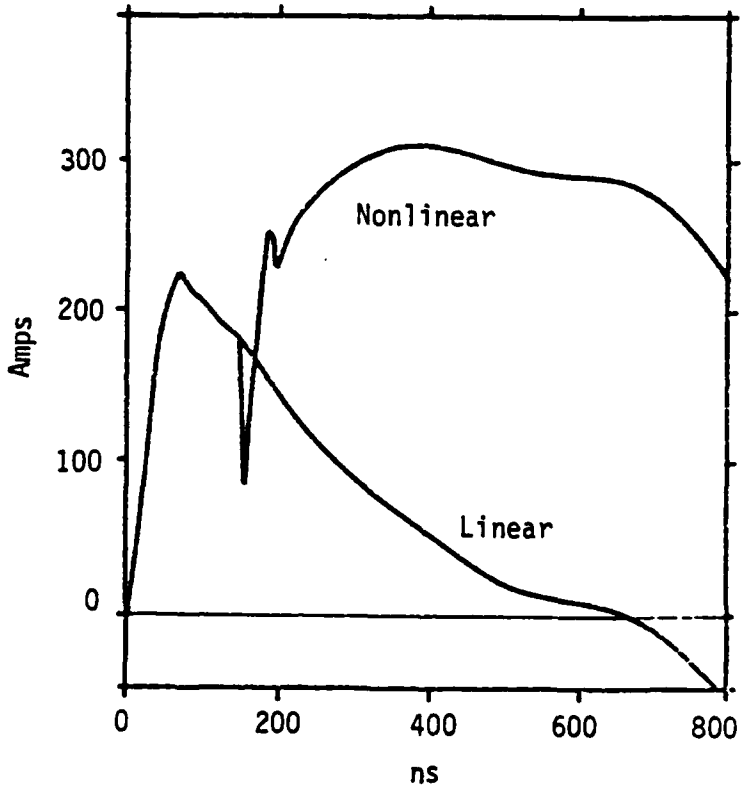

Figure 4.11 Current at Corner of "U" Cable.

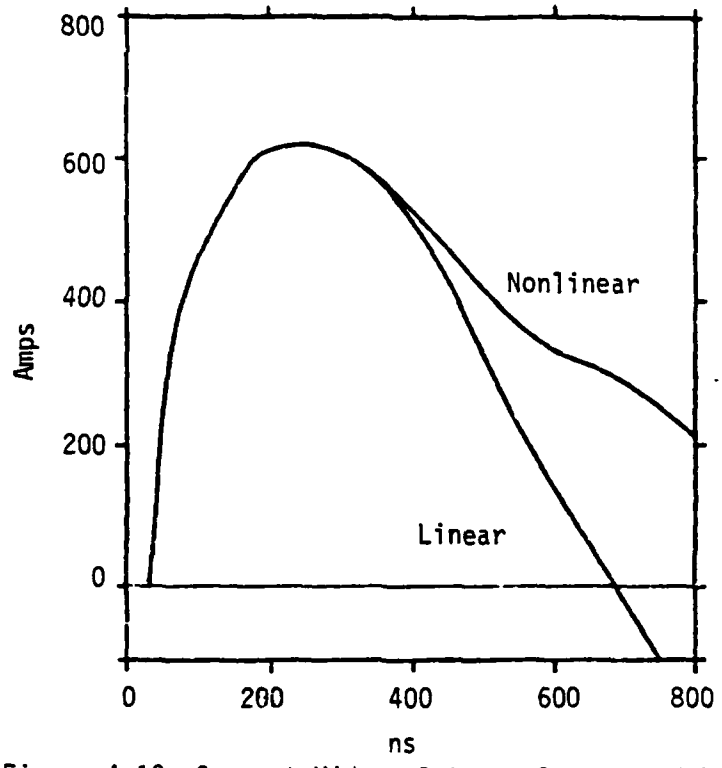

Figure 4.12 Current Midway Between Corner and End of "U" Cable.

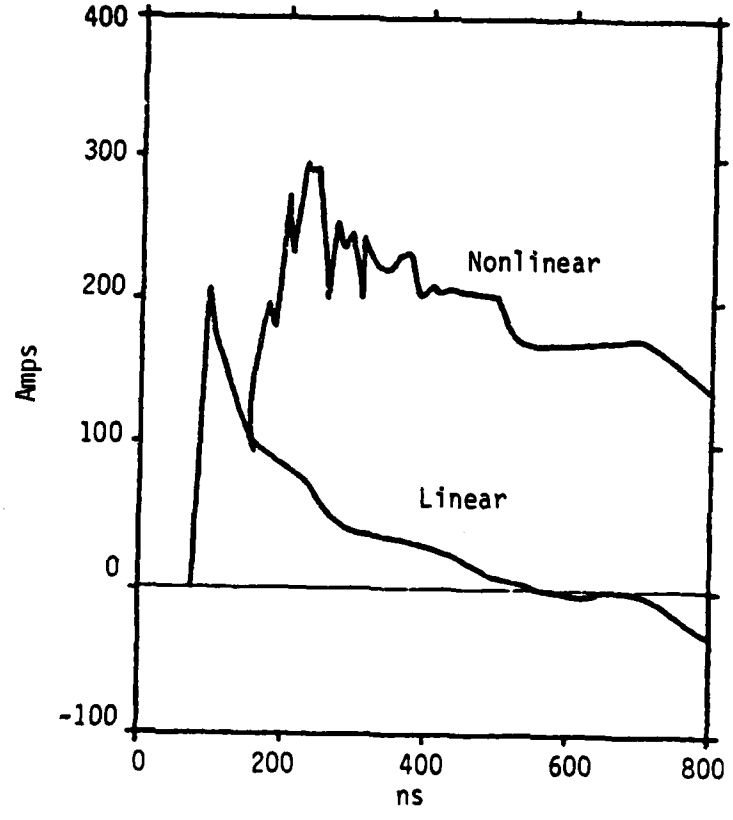

Figure 4.13 Current 1.3 Meters from the End of the "U" Cable.

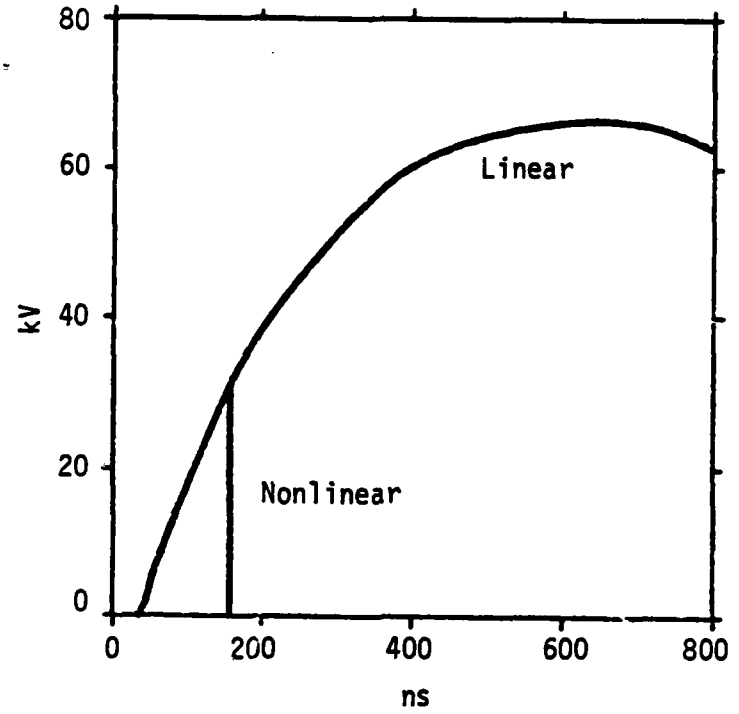

Figure 4.14 "U" Cable Corner Dielectric Voltage.

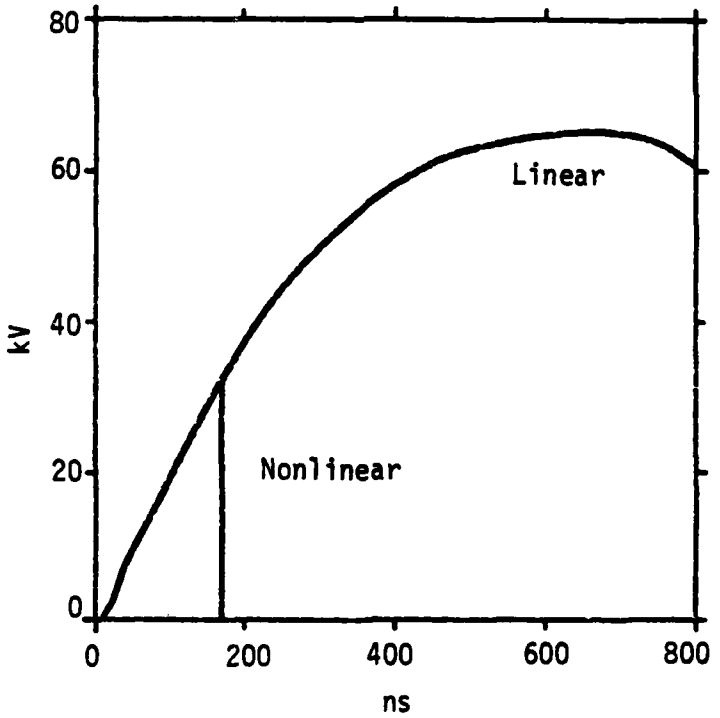

Figure 4.15 "U" Cable Center Dielectric Voltage.

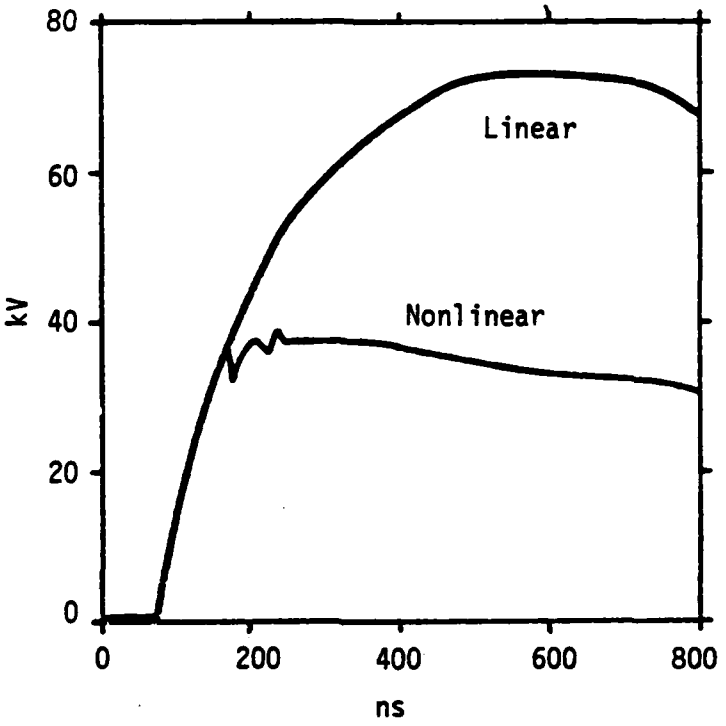

Figure 4.16 "U" Cable End Dielectric Voltage.

For the "U" cable, the punctures are in the vicinity of the corners and at the open ends. At each open end, a puncture occurs at 155 ns and punctures propagate away from the end a distance of 2.6 m, where the last puncture occurs at 491 ns, (time measured from when the incident wave arrives at the corner of the "U"). In the cable region between the two corners there are numerous punctures which occur between 153 ns and 177 ns. It is interesting to note that no punctures propagate away from the corners towards the open ends.

SECTION 5

CONCLUSIONS

This is the first known attempt to estimate the effects of soil and dielectric breakdown upon surface cable transient response, and the results need to be subjected to careful experimental comparisons. However, the analytical results indicate several interesting conclusions:

1) The effect of nonlinearities is principally to greatly increase the late time currents and reduce the voltage delivered by a cable (for the tactical case). This means that the effect of nonlinearities on system response is to reduce the voltage on high impedance systems and to increase the current on low impedance systems. Of course, a high impedance system may itself break down and become a low impedance system.

2) HAB results were not greatly affected by nonlinearities, at least for the cables studied. More dramatic effects might be observed on wires with thinner insulation, such as field wire.

3) The most important nonlinearity is cable dielectric breakdown, whereas soil breakdown is of minor, and sometimes negligible, importance.

4) The results clearly show that nonlinear air breakdown will occur in the vicinity of the cable for both HAB and tactical excitations. This effect should be evaluated as a next step, especially before performing experiments in TEMPS or AESOP.

5) One of the most important unknowns is the dielectric breakdown of cable insulations in the appropriate time regime. Data from the literature and handbooks is incomplete and conflicting. It is felt that the parties concerned should take their own data in order to have confidence in it.

6) AESOP or TEMPS can be used to validate the nonlinear analysis tools used in this study. Computations show that the important features of nonlinear cable response, such as the late time large current and the relative importance of the soil/dielectric breakdown, can be determined.

7) It is noted that results were presented for a cable "ideally" located at the earth's surface. In reality, a cable will perhaps be touching the earth's surface at only randomly selected points, and will be slightly elevated for random intervals. Results should be computed for other representative geometries.

It should be pointed out that there are several assumptions in the model which may require further research or verifications. Among these are:

1. The value for the soil breakdown fields.
2. The temporal behavior of soil breakdown (that is, it was assumed that the soil broke down without time delay, once the field exceeded the breakdown value).
3. *The validity of the "disc model".*
4. The "disc" radius was limited to be one-half of a spatial finite difference increment.
5. The value of the cable dielectric breakdown fields and their temporal dependence.
6. The validity of the model used for soil breakdown when the dielectric did not. (Surface flashover was not assumed.)
7. The accuracy of replacing f by 2/t in the skin depth formulas (Equation 2.18).

REFERENCES

1. Hill, J. R. and Wilson, M. R., "Buried Cable Transmission Line Parameters: A Comparison of Two Theoretical Models," Mission Research Corporation, AMRC-N5, March, 1973.

2. Wilson, M. R. and Merewether, D. E., "Transient Currents on Surface Cables: 2-D Finite Difference Calculations," Mission Research Corporation, AMRC-R-9, May, 1973.

3. Wilson, M. R., "Transient Current Estimate for Finite Length Surface Cables," Mission Research Corporation, AMRC-R-12, May, 1973.

4. Marston, D. R., and Graham, W. R., "Currents Induced in Cables in the Earth by a CW Electromagnetic Field," AFWL EMP Interaction Note No. 24, Vol. 2, 1966.

5. Merewether, D. E., "The Effects of Dielectric Breakdown and Soil Nonlinearities on the Response of Buried Cables to Intense Electromagnetic Pulses," Electro Magnetic Applications, Inc., EMA-78-R-1, February 1, 1978.

6. Merewether, D. E., "Analytical Model for Buried Cable Soil Breakdown Parameters," Electro Magnetic Applications, Inc., EMA-77-N-1, November, 1977.

7. Fisher, R., "BRKDWN3 Three-Dimensional Nonlinear Cable Breakdown Code Documentation and Results," Electro Magnetic Applications, Inc., EMA-78-R-4, July 21, 1978.

8. Hill, J. R. and Holland, R., "Models for EMP Coupling to Buried Cables Including Dielectric Breakdown," Mission Research Corporation, AMRC-R-44, April, 1975.

9. Vance, E. F., Electromagnetic Pulse Handbook for Electric Power Systems, Defense Nuclear Agency, DNA 3466F, 4 February, 1975.

10. Sunde, E. D., Earth Conduction Effects in Transmission Systems, Dover, N.Y., 1968.

11. Belden Electronic Wire and Cable, 1978 Catalog, Belden Corporation, Richmond, Indiana.

12. Fink, Donald G., Electronics Engineers Handbook, McGraw-Hill, 1975.

13. Reference Data for Radio Engineers, Howard Sams Publications, 1978.

14. Handbook of Tables for Applied Engineering Science, 2nd Edition, Chemical Rubber Corporation Press, Cleveland, Ohio, 1973.

15. Buschbaum, W. H., Buschbaum's Complete Handbook of Practical Electronic Reference Data, Prentice-Hall, Englewood Cliffs, N.J., 1973.

16. Von Hippel, Arthur R., Ed., Dielectric Materials and Applications, Techology Press of M.I.T. and John Wiley & Jones, New York, 1954.

17. Perala, R. A., "Further Considerations on the Lightning Susceptibility of Seafarer TAR and JSS Candidate Antenna Cables," Mission Research Corporation, AMRC-N-54 (Revised), May, 1978.

18. Newman, M. M., and Robb, J. D., "High Voltage Pulse Characteristics of Coaxial Cables," Lightning and Transient Research Institute, Minneapolis, Minnesota, L&T No. 490, July, 1968.

19. Leib, J., and Perala, R. A., "Alternative EMP Test Techniques for Underground Facilities," EG&G, Albuquerque, N.M., AL-1240, 20 September, 1976.

20. Jordan, E. C., and Balmain, K. G., Electromagnetic Waves and Radiating Systems, Prentice-Hall, N.J., 2nd Edition, 1968.

21. Stratton, J. A., Electromagnetic Theory, McGraw-Hill, New York, 1941.

ASSISTANT TO THE SECRETARY OF DEFENSE
ATOMIC ENERGY
ATTN MILITARY APPLICATIONS
ATTN EXECUTIVE ASSISTANT
WASHINGTON, DC 20301

DIRECTOR
DEFENSE COMMUNICATIONS AGENCY
ATTN CODE 312
ATTN CODE C313
ATTN CODE 430, PARKER
WASHINGTON, DC 20305

DEFENSE COMMUNICATIONS ENGINEER CENTER
1860 WIEHLE AVE
ATTN CODE R400
ATTN CODE R123, TECH LIB
RESTON, VA 22090

DIRECTOR
DEFENSE INTELLIGENCE AGENCY
ATTN DB 4C2, D. SPOHN
ATTN RTS-2A, TECH LIB
WASHINGTON, DC 20301

DIRECTOR
DEFENSE NUCLEAR AGENCY
ATTN NATA
ATTN TITL (4 COPIES)
ATTN RAEV
ATTN RAEE, G. BAKER (10 COPIES)
ATTN STNA
WASHINGTON, DC 20305

ADMINISTRATOR
DEFENSE TECHNICAL INFORMATION CENTER
ATTN DTIC-DDA (12 COPIES)
CAMERON STATION
ALEXANDRIA, VA 22314

JOINT CHIEFS OF STAFF
ATTN J-3 RM 2D874
WASHINGTON, DC 20301

NATIONAL COMMUNICATIONS SYSTEM
OFFICE OF THE MANAGER
DEPARTMENT OF DEFENSE
ATTN NCS-TS
WASHINGTON, DC 20305

DIRECTOR
NATIONAL SECURITY AGENCY
ATTN TDL
ATTN R-52, O. VAN GUNTEN
ATTN S-232, D. VINCENT
FT GEORGE G. MEADE, MD 20755

COMMANDER
BMD SYSTEMS COMMAND
DEPARTMENT OF THE ARMY
ATTN BMDSC-AOLIB
ATTN BMDSC-HLE, R. WEBB
PO BOX 1500
HUNTSVILLE, AL 35807

DIVISION ENGINEER
US ARMY ENGR. DIV. HUNTSVILLE
ATTN T. BOLT
PO BOX 1600, WEST STATION
HUNTSVILLE, AL 35807

DIRECTOR
US ARMY BALLISTIC RESEARCH LABS
ATTN DRDAR-BLB, W. VAN ANTWERP
ATTN DRDAR-BLE
ABERDEEN PROVING GROUND, MD 21005

COMMANDER
US ARMY COMMUNICATIONS COMMAND
ATTN CC-LOG-LEO
ATTN CC-OPS-WS, CONNELL
ATTN CC-OPS-PD
ATTN CC-OPS-OS
ATTN ATSI-CD-MD
FT HUACHUCA, AZ 85613

CHIEF
US ARMY COMMUNICATIONS SYS AGENCY
DEPARTMENT OF THE ARMY
ATTN CCM-AD-SV
ATTN CCM-RD-T
FT MONMOUTH, NJ 07703

COMMANDER
US ARMY NUCLEAR & CHEMICAL AGENCY
ATTN MONA-WE
ATTN DR. BERBERET
7500 BACKLICK ROAD
BUILDING 2073
SPRINGFIELD, VA 22150

COMMANDER
US ARMY TRAINING AND DOCTRINE COMMAND
ATTN ATCD-Z
FT MONROE, VA 23651

BMD CORP
ATTN CORPORATE LIBRARY
7915 JONES BRANCH DRIVE
MCLEAN, VA 22101

BENDIX CORP
COMMUNICATION DIVISION
ATTN DOCUMENT CONTROL
E JOPPA ROAD
BALTIMORE, MD 21204

DIKEWOOD CORPORATION
ATTN TECHNICAL LIBRARY
1613 UNIVERSITY BLVD, NE
ALBUQUERQUE, NM 87102

ELECTRO-MAGNETIC APPLICATIONS, INC.
ATTN D. MEREWETHER
PO BOX 8482
ALBUQUERQUE, NM 87198

GENERAL ELECTRIC CO.
SPACE DIVISION
VALLEY FORGE SPACE CENTER
ATTN J. ANDREWS
PO BOX 8555
PHILADELPHIA, PA 19101

GTE/SYLVANIA
ATTN J. KILLIAN
1 RESEARCH DRIVE
WESTBORO, MA 01581

HONEYWELL, INC.
AEROSPACE & DEFENSE GROUP
ATTN S. GRAFF
ATTN W. STEWART
13350 US HIGHWAY 19 SOUTH
CLEARWATER, FL 33516

IIT RESEARCH INSTITUTE
ELECTROMAG COMPATIBILITY ANAL CTR
ATTN ACOAT
N SEVERN
ANNAPOLIS, MD 21402

IIT RESEARCH INSTITUTE
ATTN I. MINDEL
10 W 35TH ST
CHICAGO, IL 60616

IRT CORP.
ATTN J. KNIGHTON
PO BOX 81087
SAN DIEGO, CA 92138

LUTECH, INC.
ATTN F. TESCHE
PO BOX 1263
BERKELEY, CA 94701

MARTIN MARIETTA CORP
ATTN M. GRIFFITH (2 COPIES)
ATTN J. CASALESE
ATTN B. BROULIK
PO BOX 5837
ORLANDO, FL 32855

MCDONNELL DOUGLAS CORP
ATTN S. SCHNEIDER
ATTN TECHNICAL LIBRARY SERVICES
5301 BOLSA AVE
HUNTINGTON BEACH, CA 92647

MISSION RESEARCH CORPORATION
ATTN J. RAYMOND
ATTN J. CHERVENAK
5434 RUFFIN ROAD
SAN DIEGO, CA 92123

MISSION RESEARCH CORP
ATTN W. CREVIER
ATTN C. LONGMIRE
ATTN EMP GROUP
PO DRAWER 719
SANTA BARBARA, CA 93102

MISSION RESEARCH CORPORATION
ATTN W. STARK
ATTN J. LUBELL
ATTN W. WARE
PO BOX 7816
COLORADO SPRINGS, CO 80933

RICHARD L. MONROE ASSOCIATES
1911 R STREET NW
SUITE 203
WASHINGTON, DC 20009

NORTHROP CORP.
ELECTRONIC DIVISION
ATTN LEW SMITH
ATTN RAD EFFECTS GRP
ATTN B. AHLPORT
2301 W 120TH ST
HAWTHORNE, CA 90250

R&D ASSOCIATES
ATTN DOCUMENT CONTROL
ATTN W. GRAHAM
ATTN C. MO
ATTN M. GROVER
PO BOX 9695
MARINA DEL REY, CA 90291

RAYTHEON CO
ATTN G. JOSHI
ATTN H. FLESCHER
HARTWELL ROAD
BEDFORD, MA 01730

ROCKWELL INTERNATIONAL
ATTN B-1 DIV TIC (BAOB)
PO BOX 92098
LOS ANGELES, CA 90009

SEA
MARINER SQUARE
ATTN W. HUTCHINSON
SUITE 127
1900 N. NORTHLAKE WAY
PO BOX 31819
SEATTLE, WA 98103

SRI INTERNATIONAL
ATTN E. VANCE
ATTN A. WHITSON
333 RAVENSWOOD AVE
MENLO PARK, CA 94025

TELEDYNE-BROWN ENGINEERING
ATTN D. GUICE
CUMMINGS RESEARCH PARK
HUNTSVILLE, AL 35807

TRW ELECTRONICS AND DEFENSE SYSTEMS GROUP
ATTN W. GARGARO
ATTN L. MAGNOLIA
ATTN R. PLEBUCH
ATTN C. ADAMS
ATTN H. HOLLOWAY
ATTN E. HORGAN
ATTN J. PENAR
ONE SPACE PARK
REDONDO BEACH, CA 90278

HARRY DIAMOND LABORATORIES
ATTN CO/TD/TSO/DIVISION DIRECTORS
ATTN RECORD COPY, 81200
ATTN HDL LIBRARY, 81100 (3 COPIES)
ATTN HDL LIBRARY, 81100 (WOODBRIDGE)
ATTN TECHNICAL REPORTS BRANCH, 81300
ATTN CHAIRMAN, EDITORIAL COMMITTEE
ATTN LEGAL OFFICE, 97000
ATTN BRANCH 20000
ATTN BRANCH 20240 (10 COPIES)
ATTN BRANCH 21100
ATTN BRANCH 21200
ATTN BRANCH 21300 (10 COPIES)
ATTN BRANCH 21400
ATTN BRANCH 21500
ATTN BRANCH 21000
ATTN BRANCH 22000
ATTN BRANCH 22300 (2 COPIES)
2800 POWDER MILL RD
ADELPHI, MD 20783

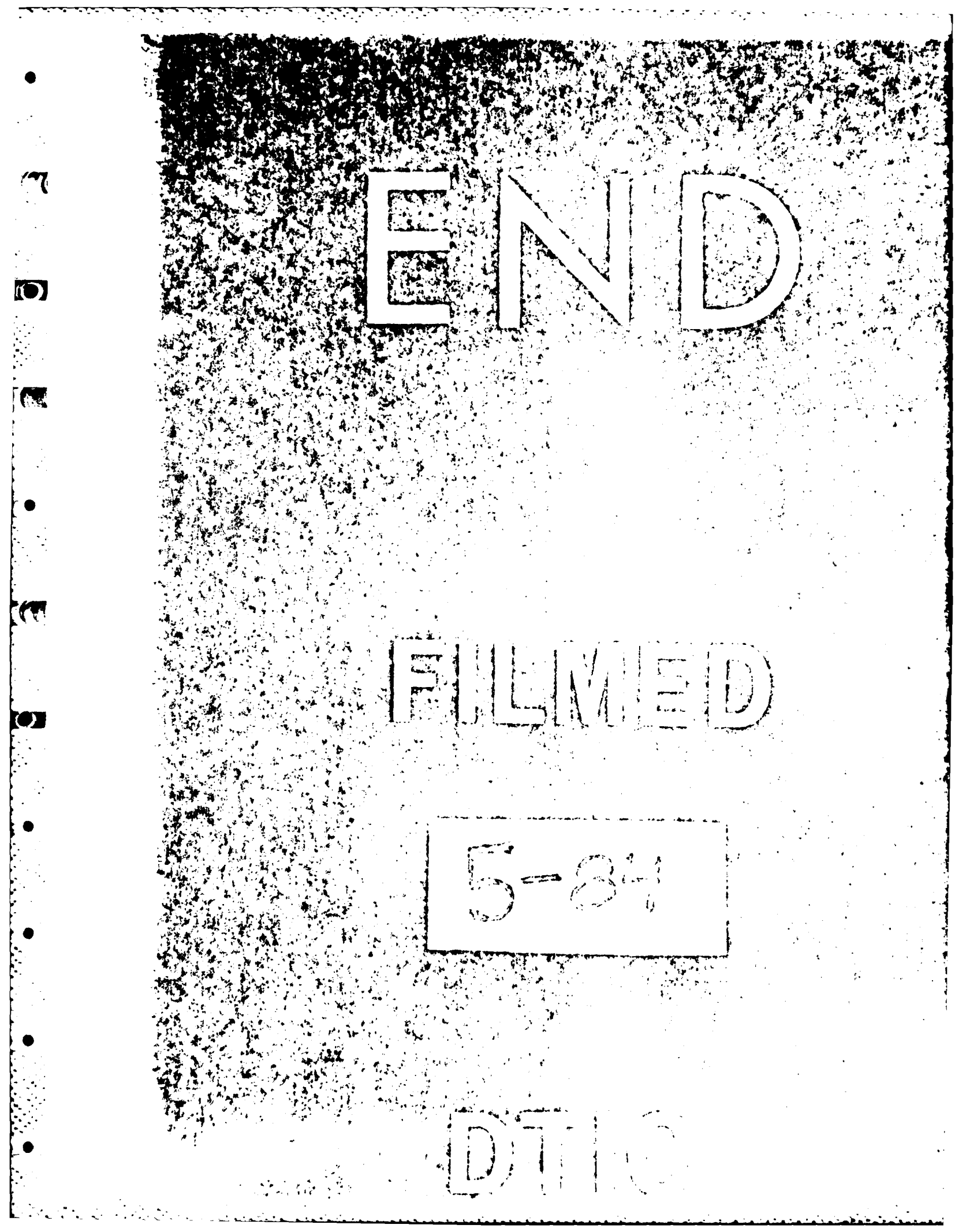
END
FILMED
5-84
DTIC